

Interacting topological Dirac magnons

Hao Sun,^{1,*} Dhiman Bhowmick,¹ Bo Yang,^{1,2,†} and Pinaki Sengupta^{1,‡}

¹*School of Physical and Mathematical Sciences, Nanyang Technological University, 21 Nanyang Link, Singapore 637371, Singapore*

²*Institute of High Performance Computing, A*STAR, Singapore 138632, Singapore*

(Dated: July 11, 2022)

In this work, we study the magnon-magnon interaction effect in typical honeycomb ferromagnets consisting of van der Waals-bonded stacks of honeycomb layers, e.g., chromium trihalides CrX₃ (X = F, Cl, Br and I), that display two spin-wave modes (Dirac magnon). Using Green's function formalism with the presence of the Dzyaloshinskii-Moriya interaction, we obtain a spinor Dyson equation up to the second-order approximation by the cluster expansion method. Numerical calculations show prominent renormalizations of the single-particle spectrum. Furthermore, we propose a tunable renormalization effect using a parametric magnon amplification scheme. By amplifying the magnon population at different k points, the enabled renormalization effect not only reshapes the band structure but also modifies the Berry curvature distribution. Our work demonstrates the interplay between band geometry, interactions, and the external light field in the bosonic system and can potentially lead to new insights into the properties of magnon-based spintronic devices.

I. INTRODUCTION

Following the phenomenal growth in the study of Dirac fermions in graphene and other (quasi-) two dimensional materials [1–10], there has been growing interest in recent years in investigating bosonic analogs of the same [11–19]. These include both fundamental particles such as photons, as well as quasiparticles such as phonons and magnons. Magnons are low-energy quasiparticle excitations in quantum magnets and have long served as a versatile testbed for realizing bosonic analogs of fermionic phases.

Since magnetic properties are easily controlled by external magnetic fields, magnonic bands offer a unique platform to explore the rich and still evolving fundamentals of the band theory. So far, several topological magnon phases have been proposed and material candidates have been identified [20–26]. Some key results include the characterization of the Chern magnon bands and linear touching points – for example, the material Cu[1,3–bdc] with the kagome lattice exhibits a magnetic field-dependent thermal Hall conductivity, and the material Cu₃TeO₆ shows a nodal topology [27, 28].

Magnonic systems are also ideal platforms for investigating interacting bosons [15, 29]. In contrast to the fermionic quasiparticles, the absence of a conservation law for the magnon particle number allows for nonconserved many-body interactions such as spontaneous decay of magnons [29, 30]. However, so far, studies of magnonic band topology have largely neglected magnon-magnon interactions, treating the magnons within the single-particle approximation [21]. This is typically justified by the argument that interaction effects are frozen out at low temperatures or are negligible as a small perturbative effect. However, the single-particle picture does not generally apply, and interactions become important when the magnon density is enhanced – either due to increased temperature, or parametric amplification (as discussed later). In

Dirac fermions, Coulomb interaction leads to a logarithmic renormalization of the Fermi velocity [31], and similar analyses for interacting magnons have shown that both velocity and energy are renormalized due to interaction in the vicinity of the Dirac points [15].

In this work, we have investigated the effects of interactions on *topological* magnons in a Heisenberg ferromagnet with Dzyaloshinskii-Moriya interaction (DMI) on a honeycomb lattice. In the absence of DMI, the single-particle magnon spectrum features two bands that touch at the Dirac points with linear dispersion. DMI opens up a gap in the spectrum and imparts non-trivial topology to the bands. We have investigated the effects of interaction on the band topology using Green's function formalism up to the second-order in perturbation theory. Crucially, we are able to systematically probe the interaction-driven renormalization of the magnon bands in different parts of the magnetic Brillouin zone, and isolate the effects of interactions from thermal fluctuations, by employing the recently developed magnon amplification scheme to controllably tune magnon density at selective energy-momentum values [32]. Our results show that the magnon-magnon interaction leads to a significant momentum-dependent renormalization of the single-magnon dispersion – interactions suppress the bandwidth, and lead to dissipative scattering of the magnons. More interestingly, interaction effects, in conjunction with DMI and magnon amplification can introduce a non-trivial Haldane term (complex next nearest neighbor hopping) – and consequently, topological phase transition – leading to magnon bands with tunable Chern numbers. In the same vein, the Berry curvature distribution of the magnon bands can be tailored by interactions. We argue from a microscopic perspective that effective gauge fields emerge in this bipartite system through their underlying interaction, and propose that a magnon-mediated anomalous transport – the thermal Hall effect – allows for the experimental investigation of this many-body effect [33].

The remainder of this paper is structured as follows. Section II introduces the basic theory of interacting magnons. The Green's function formalism is introduced in Sec. II A. A low-temperature approximation is discussed in Sec. II B as an intuitive introduction to the band renormalization, and finally,

* sunhao@ntu.edu.sg

† yang.bo@ntu.edu.sg

‡ psengupta@ntu.edu.sg

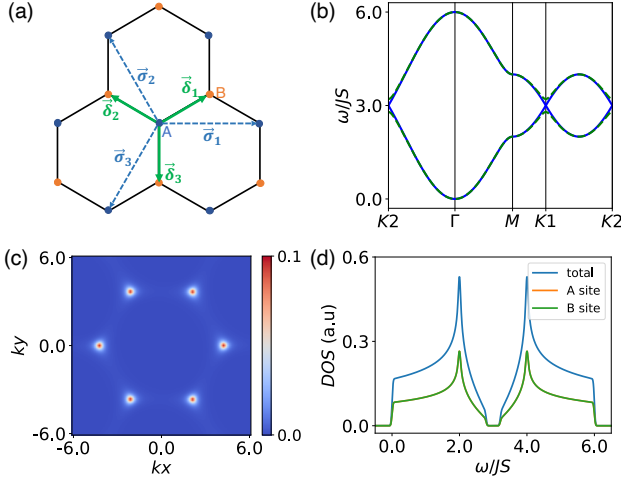


FIG. 1. Honeycomb structure of ferromagnet and noninteracting spectrum of magnonic excitation. (a) Geometric structure of honeycomb ferromagnets with NN bonds δ_n and NNN bonds σ_n . (b) Calculated magnon spectrum by single-particle Hamiltonian, dashed green curves are the topological non-trivial bands with $D/J = 0.05$. One can see the DMI-induced gaps at the Dirac points. (c) Berry curvature distribution of acoustic branch with $D/J = 0.05$. (d) The density of states and partial density of states for gapped magnon bands. One can see the conserved sublattice symmetry from the equal distributions of A and B sites.

the renormalization expression is extended beyond the low-temperature approximation in Sec. II C. Section III focuses on the main calculation results. The emergence of the gauge field and the modification of band geometry due to many-body interaction is discussed using the quantum geometric tensor in Sec. III, and the evolution of the spinor spectral function and the scattering rate with DMI using second-order self-energy is discussed in Sec. IV. Section V presents the results of magnon amplification via parametric instability and experimental feasibility of demonstrating the theoretical results in a real quantum magnet, with Sec. V A showing how the magnon population can be amplified by the external light field and Sec. V B examining the relationship between magnon populations and the thermal Hall conductivities. We end with a summary and conclusions in Sec. VI.

II. DIRAC MAGNONS IN HONEYCOMB FERROMAGNET

The Heisenberg model on the honeycomb lattice is described by the Hamiltonian:

$$H = -J \sum_{\langle ij \rangle} \mathbf{S}_i \cdot \mathbf{S}_j, \quad (1)$$

where $J > 0$ denotes the strength of ferromagnetic nearest neighbour (NN) exchange coupling and \mathbf{S}_i denotes the local spin on the i -site of the lattice. The ground state is a ferromagnet, and low energy magnon excitations above the ground state are obtained through the Holstein-Primakoff (HP) transformation [34], which reduces to the familiar linear spin-wave

theory in its lowest order:

$$S_i^x + iS_i^y = \sqrt{2S}a_i, \quad S_i^x - iS_i^y = \sqrt{2S}a_i^\dagger, \quad S_i^z = S - a_i^\dagger a_i. \quad (2)$$

a (a^\dagger) is the magnon annihilation (creation) operator, and obey commutation relation $[a_i, a_j^\dagger] = \delta_{ij}$. In the linear spin wave theory framework (neglecting any magnon-magnon interaction), the above Hamiltonian reduces to an effective tight-binding model of magnons:

$$H = -JS \sum_{\langle ij \rangle} a_i^\dagger a_j + 3JS \sum_i a_i^\dagger a_i. \quad (3)$$

Here, we have subtracted the ferromagnetic ground state energy $E_G = -3N_L JS^2$. N_L is the number of unit cells [12].

DMI in honeycomb ferromagnets is the dominant interaction driving the topological properties of the magnons. Here we introduce a physically relevant out-of-plane next nearest neighbor (NNN) DMI, $\mathbf{D}_{i'j'} \cdot (\mathbf{S}_{i'} \times \mathbf{S}_{j'}) = \sum_{\alpha\beta\gamma} D \varepsilon_{\alpha\beta\gamma} v_{ij'}^\alpha S_{i'}^\beta S_{j'}^\gamma$, where $v_{ij'}^\alpha = \frac{a_{i'j'}^1 \times a_{i'j'}^2}{|a_{i'j'}^1 \times a_{i'j'}^2|} = (0, 0, \pm 1)$, and D is the strength of the DM vector. We redefine the HP boson operator with two flavors due to the pseudospin degree of freedom: $a_i \rightarrow a_i, a_j \rightarrow b_{i+\delta_n}$. The δ_n are the three NN bonds of magnon orbital with $\delta_1 = (\frac{1}{2}, \frac{1}{2\sqrt{3}})$, $\delta_2 = (\frac{-1}{2}, \frac{1}{2\sqrt{3}})$ and $\delta_3 = (0, \frac{-1}{\sqrt{3}})$. We plot them as the green arrows shown in Fig. 1(a). Fourier transformation of Eq.(3), yields the single-magnon Hamiltonian in the momentum space: $H_0 = \sum_{\mathbf{k}} \Psi_{\mathbf{k}}^\dagger M_{\mathbf{k}} \Psi_{\mathbf{k}}$ with $\Psi_{\mathbf{k}}^\dagger = (a_{\mathbf{k}}^\dagger, b_{\mathbf{k}}^\dagger)$. The explicit expression of the H_0 is given by:

$$H_0 = \sum_{\mathbf{k}} (a_{\mathbf{k}}^\dagger, b_{\mathbf{k}}^\dagger) \begin{pmatrix} 3J - 2DS\beta_{\mathbf{k}} & -JS\gamma_{\mathbf{k}} \\ -JS\gamma_{\mathbf{k}}^* & 3JS + 2DS\beta_{\mathbf{k}} \end{pmatrix} \begin{pmatrix} a_{\mathbf{k}} \\ b_{\mathbf{k}} \end{pmatrix}, \quad (4)$$

where $\gamma_{\mathbf{k}_i} = \sum_n e^{i\mathbf{k}_i \cdot \delta_n}$, $\beta_{\mathbf{k}} = \sum_n \text{Im}(e^{i\mathbf{k} \cdot \sigma_n})$, and σ_n are the NNN bonds with $\sigma_1 = (1, 0)$, $\sigma_2 = (\frac{-1}{2}, \frac{\sqrt{3}}{2})$ and $\sigma_3 = (\frac{-1}{2}, \frac{-\sqrt{3}}{2})$. The NNN bonds are represented by the dashed blue arrows, as shown in Fig. 1(a). Using the canonical diagonalization process, we obtain the spectrum of the H_0 :

$$\omega_{\mathbf{k}} = 3JS \pm \sqrt{J^2 S^2 |\gamma_{\mathbf{k}}|^2 + 4D^2 S^2 \beta_{\mathbf{k}}^2}. \quad (5)$$

When $\mathbf{k} \rightarrow 0$, the asymptotic expression of lowest energy $\omega_{\mathbf{k}} \approx \frac{1}{2}JS\mathbf{k}^2 \rightarrow 0$ reveals the gapless nature of the magnon excitation. This gapless Goldstone mode is the consequence of the spontaneously broken symmetry in the ferromagnetic ground state. In the honeycomb lattice, magnonic excitations appear in two flavours, exhibiting a graphene-like band structure. The two bands touch linearly at the Dirac point energy when $D = 0$. A nonzero D provides an effective Haldane mass term that opens up a non-trivial band gap $\Delta g = 6\sqrt{3}DS$ between the upper and lower branches at the Dirac points. The spectra are plotted in Fig. 1(b). One can see the blue curves of the gapless bands with $D = 0$ and dashed green curves of the gapped topological bands with $D/J = 0.05$.

The Berry curvature distributions of the lower band are shown in Fig. 1(c), the finite values with the same sign around the gapped Dirac points contribute to the integer Chern number $C = 1$ by k -space integration. Similar to the corresponding fermionic systems, the non-zero Berry curvature provides an effective gauge field for the bosonic magnons in the k -space and dominates the transport properties. One should note that a small, but non-zero, magnetic field is necessary for stabilizing the ferromagnetic phase and the magnon excitations because the Mermin-Wagner theorem rules out the long-distance ferromagnetic order in 2D systems at finite temperatures without the magnetic field [35]. However, the role of the magnetic field is just to stabilize the ground state; it does not contribute to the topological properties of the bands.

A. Interaction renormalized Dirac magnon

Considering the first-order expansion of $\frac{1}{\sqrt{3}}$ in HP transformation, we include the magnon-magnon interaction in the real lattice space:

$$H' = \frac{J}{4} \sum_{i,n} a_i^\dagger b_{i+\delta_n}^\dagger b_{i+\delta_n} b_{i+\delta_n} + b_{i+\delta_n}^\dagger b_{i+\delta_n}^\dagger a_i b_{i+\delta_n} + a_i^\dagger b_{i+\delta_n}^\dagger a_i a_i + a_i^\dagger a_i^\dagger a_i b_{i+\delta_n} - J \sum_{i,n} a_i^\dagger a_i b_{i+\delta_n}^\dagger b_{i+\delta_n}. \quad (6)$$

The interacting Hamiltonian in k -space can be obtained by using a Fourier transformation of the above real space interaction Hamiltonian:

$$H' = \frac{J}{4N_L} \sum_{k_i} \gamma_{k_1} a_{k_1}^\dagger b_{k_2}^\dagger b_{k_3} b_{k_4} + \frac{J}{4N_L} \sum_{k_i} \gamma_{k_4}^* b_{k_1}^\dagger b_{k_2}^\dagger b_{k_3} a_{k_4} + \frac{J}{4N_L} \sum_{k_i} \gamma_{k_1}^* b_{k_1}^\dagger a_{k_2}^\dagger a_{k_3} a_{k_4} + \frac{J}{4N_L} \sum_{k_i} \gamma_{k_4} a_{k_1}^\dagger a_{k_2}^\dagger a_{k_3} b_{k_4} - \frac{J}{N_L} \sum_{k_i} \gamma_{k_4-k_2} a_{k_1}^\dagger b_{k_2}^\dagger a_{k_3} b_{k_4}. \quad (7)$$

The momentum is conserved in all of the above interaction terms by $\frac{1}{N_L} \sum_i e^{i(k_1+k_2-k_3-k_4)\cdot r_i} = \delta_{k_1+k_2, k_3+k_4}$. All the interaction terms can be expressed in a more compact form: $H' = \sum_{\{k_i\}} V_{k_3, k_4}^{k_1, k_2} \psi_{k_1}^\dagger \psi_{k_2}^\dagger \psi_{k_3} \psi_{k_4}$, where the summation runs over all (k_1, k_2, k_3, k_4) combinations constrained by the momentum conservation.

We employ a retarded Green's function formalism to study the renormalization of the magnon bands due to magnon-magnon interactions. In the real space-time domain, a retarded Green's function is defined as $\langle \psi(\mathbf{r}, t); \psi^\dagger(\mathbf{r}', t') \rangle = -i\theta(t-t') \langle [\psi(\mathbf{r}, t), \psi^\dagger(\mathbf{r}', t')] \rangle$. Here $\langle \dots \rangle$ denotes the ensemble average, $\theta(t-t')$ is the step function, and $\psi^\dagger(\mathbf{r}, t)$ is the field operator of the spinor which can be written as $(\sum_i \phi_{a,i}^*(\mathbf{r}) a_i^\dagger(t), \sum_i \phi_{b,i}^*(\mathbf{r}) b_i^\dagger(t))$. The HP boson operators of (A, B)-site in the bipartite honeycomb lattice are given by $a_i^\dagger(t)$ and $b_i^\dagger(t)$. The frequency-dependent retarded Green's function in k -space is given by $G_R(\mathbf{k}, \mathbf{k}'; \omega) = \langle \psi_{\mathbf{k}}; \psi_{\mathbf{k}'}^\dagger \rangle_\omega$.

Using the Heisenberg picture, we write down the equation of motion of Green's function in the frequency domain:

$$\omega G_R(\mathbf{k}, \mathbf{k}'; \omega) = \delta_{\mathbf{k}, \mathbf{k}'} + \langle [\psi_{\mathbf{k}}, H_0]; \psi_{\mathbf{k}'}^\dagger \rangle_\omega + \langle [\psi_{\mathbf{k}}, H']; \psi_{\mathbf{k}'}^\dagger \rangle_\omega, \quad (8)$$

where $[\psi_{\mathbf{k}}, H'] = \sum_{\{k_i\}} V_{k_3, k_4}^{(k, k_2)} \psi_{k_2}^\dagger \psi_{k_3} \psi_{k_4}$, which gives rise to many-body effects. In order to solve the above equation, we employ the mean-field approximation (MFA) and random phase approximation (RPA): $b_{k_2}^\dagger a_{k_3} b_{k_4} \approx \delta_{k_2, k_3} \langle b_{k_2}^\dagger a_{k_3} \rangle b_{k_4} + \delta_{k_2, k_4} \langle b_{k_2}^\dagger b_{k_4} \rangle a_{k_3}$. The δ -function is for the RPA, and a short explanation of its validity is in order here. Generally, the expectation value $\langle b_{k_2}^\dagger a_{k_3} \rangle$ has a dominant time dependence $\langle b_{k_2}^\dagger a_{k_3} \rangle \propto e^{i(\omega_{k_2} - \omega_{k_3})t}$. When considering summation over all k_2 and k_3 , we neglect the terms with $k_2 \neq k_3$, because these are averaged to zero due to the rapid oscillations in the time domain, and therefore we only retain the dominant contribution from $k_2 = k_3$ term.

From the perturbation theory, we can derive the spinor Dyson equation for the interacting magnons up to the second order, which is written as:

$$G_R(\mathbf{k}, \mathbf{k}'; \omega) = G_R^{(0)}(\mathbf{k}, \mathbf{k}'; \omega) + G_R^{(0)}(\mathbf{k}, \mathbf{k}'; \omega) \Sigma_{\mathbf{k}}^{(1)} G_R^{(0)}(\mathbf{k}, \mathbf{k}'; \omega) + G_R^{(0)}(\mathbf{k}, \mathbf{k}'; \omega) \Sigma_{\mathbf{k}}^{(2)}(\omega) G_R^{(0)}(\mathbf{k}, \mathbf{k}'; \omega), \quad (9)$$

where $G_R(\mathbf{k}, \mathbf{k}'; \omega)$ is the interacting spinor Green's function of the Dirac magnon, $G_R^{(0)}(\mathbf{k}, \mathbf{k}'; \omega) = \frac{\delta_{\mathbf{k}, \mathbf{k}'}}{\omega - M(\mathbf{k}'})$ is the free particle Green's function without magnon-magnon interactions. $\Sigma_{\mathbf{k}}^{(1)}$ and $\Sigma_{\mathbf{k}}^{(2)}$ are the first-order and second-order self-energies, respectively. We will show the explicit forms in the following sections.

Using MFA and RPA, we can simply expand $[\psi_{\mathbf{k}}, H']$ in Eq. (8), and obtain the Hartree-type self-energy, which is the first-order renormalization given by:

$$\Sigma_{H'}^{(1)}(\mathbf{k}) = \sum_{k_2} V_{(k_2, \mathbf{k})}^{(k, k_2)} \langle \psi_{k_2}^\dagger \psi_{k_2} \rangle^{(0)}, \quad (10)$$

where $V_{(k_2, \mathbf{k})}^{(k, k_2)} = 2V_{k_2, \mathbf{k}}^{k, k_2} + 2V_{\mathbf{k}, k_2}^{k, k_2}$ is the interaction coefficient matrix, $\langle \psi_{k_2}^\dagger \psi_{k_2} \rangle^{(0)} = \begin{pmatrix} \langle a_{k_2}^\dagger a_{k_2} \rangle^{(0)} & \langle a_{k_2}^\dagger b_{k_2} \rangle^{(0)} \\ \langle b_{k_2}^\dagger a_{k_2} \rangle^{(0)} & \langle b_{k_2}^\dagger b_{k_2} \rangle^{(0)} \end{pmatrix}$ is the zeroth order population matrix, which is basically determined by the thermal excitation or the magnon parametric amplifications [32, 36].

B. Low temperature approximation

In the case of thermal excitation we usually use a low temperature approximation, which means that we only include finite density magnonic excitations around the lowest energy state at Γ point in the lower magnon band. The first-order self-energy $\Sigma_{\mathbf{k}}^{(1)}$ of the thermal excitation is given by [15]:

$$\Sigma_{H'}^{(1)}(\mathbf{k}) \approx -\frac{J}{2N_L} \sum_{k_1} \frac{\omega_{k_1}}{3JS} f(\omega_{k_1}) \begin{pmatrix} 3 & -\gamma_{\mathbf{k}} \\ -\gamma_{\mathbf{k}}^* & 3 \end{pmatrix}, \quad (11)$$

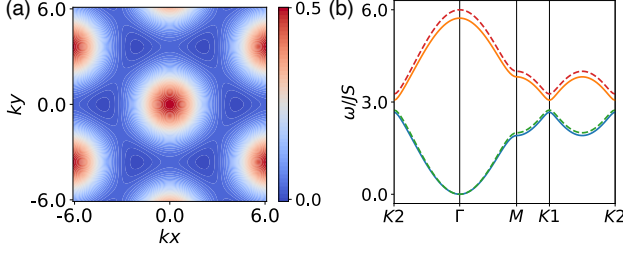


FIG. 2. The first order renormalization on magnon band from thermal excitation. (a) The density of renormalization factor $a^T(\mathbf{k})$, where $\int_{BZ} d^2\mathbf{k} a^T(\mathbf{k}) = \alpha(T)$. (b) Renormalized magnon bands at $k_B T/JS = 0.8$ are shown by solid curves, which have smaller band widths compared to the pristine magnon bands in dashed curves.

where $f(\omega_{\mathbf{k}_1}) = \frac{1}{e^{\omega_{\mathbf{k}_1}/\beta} - 1}$ is the Bose-Einstein distribution of magnons at finite temperature T , and $\beta = \frac{1}{k_B T}$. We employ the quadratic approximation $\omega_{\mathbf{q}} \approx c_2 q^2$ of the acoustic magnon band around the Γ point. The summation $\frac{1}{N_L} \sum_{\mathbf{q}} \omega_{\mathbf{q}} f(\omega_{\mathbf{q}})$ in the above equation can be easily evaluated, and we obtain $\frac{1}{N_L} \sum_{\mathbf{q}} c_2 q^2 \frac{1}{e^{\omega_{\mathbf{q}}/\beta} - 1} = \frac{A k_B^2}{4\pi c_2} \zeta(2) T^2$, where A is the area of the primitive unit cell, and $\zeta(2)$ is the Riemann zeta function. Finally, we have a renormalized magnon band modified by the first-order self-energy:

$$\omega_{\mathbf{k}} = 3JS(1 - \alpha(T)) \pm \sqrt{(1 - \alpha(T))^2 J^2 S^2 |\gamma_{\mathbf{k}}|^2 + 4D^2 S^2 \beta_{\mathbf{k}}^2}, \quad (12)$$

where $\alpha(T) = \frac{A\pi k_B^2}{24J^2 S^3} T^2 \propto T^2$ is defined as the renormalization factor, which is consistent with the results in [15] (also see Appendix B). We plot the distribution of the renormalization factor from the thermal excitation at $k_B T/JS = 0.8$ in Fig. 2(a), and the modified magnon band in Fig. 2(b). The first-order renormalization at a low temperature ($T \ll J$) does not change the non-trivial magnon gap, but does reduce the magnon bandwidth by a factor $1 - \alpha(T)$.

C. Beyond the low temperature approximation

The above discussion is only valid at low temperatures. The thermally generated magnons are concentrated at the bottom of the band where the Berry curvature is minimum. As a result, the effects of non-trivial band topology are not manifested in any physical observable. Fortunately, recent studies have shown that magnons can be excited not only by thermal energy but also at any energy-momentum point of the spectrum by an external electromagnetic field [32]. Hence one can controllably generate magnons at specific points in the magnetic Brillouin zone with a large concentration of Berry curvature so that the simultaneous effects of non-trivial band topology and interactions on magnons can be studied systematically. This is the approach taken in the following. To encompass all possible situations, we shall focus on the full expression of the first-order self-energy from the interacting

Hamiltonian:

$$\Sigma_{H'}^{(1)}(\mathbf{k}) = \frac{J}{2N_L} \sum_{\mathbf{k}_1} \begin{pmatrix} |\gamma_{\mathbf{k}_1}| \Delta_2(\mathbf{k}_1) - \gamma_0 \Theta_b(\mathbf{k}_1) & \gamma_{\mathbf{k}} \Theta^+(\mathbf{k}_1) - \theta(\mathbf{k}, \mathbf{k}_1) \\ \gamma_{\mathbf{k}}^* \Theta^+(\mathbf{k}_1) - \theta^*(\mathbf{k}, \mathbf{k}_1) & |\gamma_{\mathbf{k}_1}| \Delta_2(\mathbf{k}_1) - \gamma_0 \Theta_a(\mathbf{k}_1) \end{pmatrix}, \quad (13)$$

where we have the terms:

$$\begin{aligned} \Delta_2(\mathbf{k}_1) &= \sqrt{1 - \frac{B^2}{A^2}} \Theta^-(\mathbf{k}_1), \\ \Theta_b(\mathbf{k}_1) &= \Theta^+(\mathbf{k}_1) - \frac{B}{A} \Theta^-(\mathbf{k}_1), \\ \Theta_a(\mathbf{k}_1) &= \Theta^+(\mathbf{k}_1) + \frac{B}{A} \Theta^-(\mathbf{k}_1), \\ \theta(\mathbf{k}, \mathbf{k}_1) &= \Delta_2(\mathbf{k}_1) \gamma_{\mathbf{k}-\mathbf{k}_1} e^{i\phi_{\mathbf{k}_1}}, \end{aligned} \quad (14)$$

and $A = \sqrt{(2D\beta_{\mathbf{k}})^2 + |\gamma_{\mathbf{k}}|^2}$, $B = \frac{2D\beta_{\mathbf{k}}}{J}$, $\Theta^+(\mathbf{k}) = f(\omega_{d_{\mathbf{k}}}) + f(\omega_{u_{\mathbf{k}}})$, $\Theta^-(\mathbf{k}) = f(\omega_{d_{\mathbf{k}}}) - f(\omega_{u_{\mathbf{k}}})$, $f(\omega_{d_{\mathbf{k}}})$ and $f(\omega_{u_{\mathbf{k}}})$ are the magnon populations at point \mathbf{k} of lower and upper bands, respectively. The quartic DM interactions are also considered, leading to a self-energy term given by $\Sigma_{DM}^{(1)}(\mathbf{k}) = \begin{pmatrix} \sigma'_{11} & 0 \\ 0 & \sigma'_{22} \end{pmatrix}$. The explicit form of each term is (more details in Appendix B):

$$\begin{aligned} \sigma'_{11} &= \frac{D\beta_{\mathbf{k}}}{N_L} \sum_{\mathbf{k}_1} \Theta^+(\mathbf{k}_1) + \frac{D}{N_L} \sum_{\mathbf{k}_1} \frac{\beta_{\mathbf{k}_1} B}{A} \Theta^-(\mathbf{k}_1) \\ \sigma'_{22} &= -\frac{D\beta_{\mathbf{k}}}{N_L} \sum_{\mathbf{k}_1} \Theta^+(\mathbf{k}_1) + \frac{D}{N_L} \sum_{\mathbf{k}_1} \frac{\beta_{\mathbf{k}_1} B}{A} \Theta^-(\mathbf{k}_1). \end{aligned} \quad (15)$$

Hence the renormalized Hamiltonian at the first-order level is given by:

$$\begin{aligned} H_1 &= H_0 + \Sigma_{H'}^{(1)}(\mathbf{k}) + \Sigma_{DM}^{(1)}(\mathbf{k}) \\ &= \begin{pmatrix} 3JS - 2DS\beta_{\mathbf{k}} + P + \delta_m & -(JS - Q)\gamma_{\mathbf{k}} - g(\mathbf{k}) \\ -(JS - Q)\gamma_{\mathbf{k}}^* - g^*(\mathbf{k}) & 3JS + 2DS\beta_{\mathbf{k}} + P - \delta_m \end{pmatrix}, \end{aligned} \quad (16)$$

where $P = \frac{J}{2N_L} \sum_{\mathbf{k}_1} (\Delta_1(\mathbf{k}_1) - \gamma_0 \Theta^+(\mathbf{k}_1))$, $\Delta_1(\mathbf{k}_1) = |\gamma_{\mathbf{k}_1}| \Delta_2(\mathbf{k}_1) + \frac{B^2}{A} \Theta^-(\mathbf{k}_1)$, and $Q = \frac{J}{2N_L} \sum_{\mathbf{k}_1} \Theta^+(\mathbf{k}_1)$. These are all overall factors and \mathbf{k} -independent. It is easy to see that the diagonal term P mimics the scalar potential, and the interaction-induced off-diagonal term $g(\mathbf{k}) = \frac{J}{2N_L} \sum_{\mathbf{k}_1} \theta(\mathbf{k}, \mathbf{k}_1)$ mimics the vector potential in the vicinity of the magnon Dirac point using minimal coupling with $\gamma_{\mathbf{k}} + g(\mathbf{k}) \rightarrow \mathbf{k} + g(\mathbf{k}_D)$.

The most interesting term is the interaction-induced Haldane term $\delta_m = \frac{J}{2N_L} B(\mathbf{k}) \sum_{\mathbf{k}_1} \Theta^+(\mathbf{k}_1)$. Thus the interaction effect can be seen as the emergent gauge field in the weakly interacting magnon system. The summation of the value \mathbf{k}_1 is limited to the first Brillouin zone. We diagonalize the new Hamiltonian to obtain the renormalized magnon spectrum as:

$$\omega_{\mathbf{k}} = 3JS + P \pm \sqrt{|(JS - Q)\gamma_{\mathbf{k}} + g(\mathbf{k})|^2 + (2DS\beta_{\mathbf{k}} - \delta_m)^2} \quad (17)$$

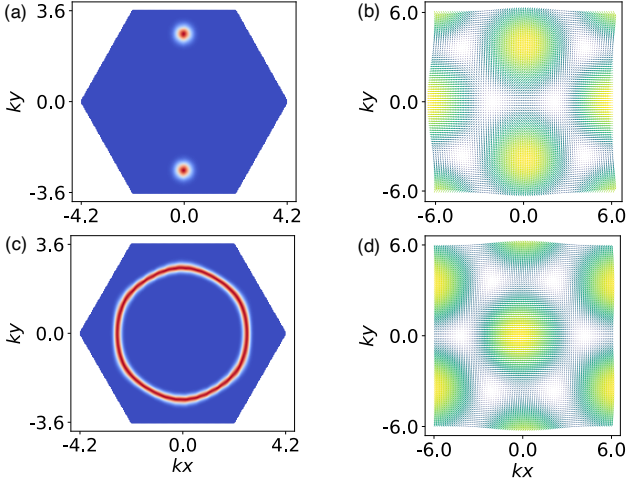


FIG. 3. Population of excited magnon by electromagnetic field and distribution of $g(\mathbf{k})$. (a) The anisotropic population of magnon by EM field amplification. Two excited magnon states with opposite \mathbf{k} vectors $((0, b)$ and $(0, -b)$). (b) Distribution of the in-plane components of the vector \mathbf{g} shows the nonuniform of $g(\mathbf{k})$ in BZ. (c) The isotropic population of magnon by EM field amplification. (d) Distribution of the in-plane components of the vector \mathbf{g} by isotropic populations in (c).

where the factor Q affects the bandwidths of the magnon consistent with the results in [15], when using a low temperature approximation.

III. BAND ENGINEERING FROM MAGNON-MAGNON INTERACTION

A. Shifting of Dirac points and quantum geometric tensor

We use Eqs.(16) and (17) to study the many-body effect for arbitrary magnon populations, in particular for magnons amplified by the electromagnetic field. The magnon amplification will be discussed in Sec. V. We argue that the treating the interaction within a mean-field theory gives rise to an effective potential, in which the diagonal part P is a scalar potential, and the off-diagonal part $g(\mathbf{k})$ is an effective vector potential in the vicinity of the Dirac point. The scalar potential P for the energy shift will not change the physics around the Dirac point.

It is interesting that in the pseudospin space, $g(\mathbf{k})$ acts as an effective in-plane Zeeman field on sublattice pseudospin σ . In Eq. (16), we can rewrite the non-trivial part as $\begin{pmatrix} \delta_m & -g(\mathbf{k}) \\ -g^*(\mathbf{k}) & -\delta_m \end{pmatrix} = \mathbf{g} \cdot \sigma$. It follows that we can reformulate the complex quantity $g(\mathbf{k})$ and the interaction-induced Haldane mass into a vector form given by the expression $\mathbf{g} = (-\text{Re}(g(\mathbf{k})), \text{Im}(g(\mathbf{k})), \delta_m)$. For an anisotropic magnon density distribution $f(\omega_{\mathbf{k}})$ as shown in Fig. 3(a), we have the distribution of vector \mathbf{g} , showing a nonuniform vortex feature illustrated in Fig. 3(b). $g(\mathbf{k})$ breaks the C_6 rotational sym-

metry of the first BZ, and as a consequence the Dirac point will be shifted by the effective vector potential, as shown in Fig. 4(a) [37]. The black dots represent the original Dirac points, whereas the red dots are the new ones shifted by \mathbf{g} . However, the gapless feature of Dirac point will still be preserved without DM interactions, since the original interaction terms in Eq (7) do not contain the symmetry breaking factors, e.g., broken time reversal and chiral symmetries. In addition, we do not include the anomalous pairing term $\langle \psi_{\mathbf{k}}^\dagger \psi_{-\mathbf{k}}^\dagger \rangle$ ($\langle \psi_{\mathbf{k}} \psi_{-\mathbf{k}} \rangle$) in RPA, which breaks the $U(1)$ symmetry. Dirac point shifts are observed in many cases by strain engineering [38, 39], whereas we propose that many-body effects can induce the same effect without lattice deformation.

The shift of Dirac points results in the change of geometric properties of the magnon dispersion. We study how the effective gauge field $g(\mathbf{k})$ modifies the geometric properties encoded in quantum geometric tensor (QGT). QGT consists of the Berry curvature and the quantum metric measuring the "distance" between the eigenstates in the Hilbert space. It is defined as follows:

$$Q_{ab} = G_{ab} - \frac{i}{2} \Omega_{ab}, \quad (18)$$

where the real part G_{ab} is the quantum metric, and Ω_{ab} is the Berry curvature. We already know that Berry curvature is crucial for topological phases; the quantum metric is associated with superfluidity in flat bands and orbital magnetic susceptibility. Finally, it should be noted that the QGT is not just an abstract mathematical construct, but has been measured directly [40]. Since the gauge-invariant QGT contains the structural information about the eigenstates of a parametrized Hamiltonian, we have the explicit expressions as below:

$$G_{ab} = \text{Re} \left(\sum_{m \neq n} \frac{\langle u_m | \partial_{k_a} H | u_n \rangle \langle u_n | \partial_{k_b} H | u_m \rangle}{(E_m - E_n)^2} \right),$$

$$\Omega_{ab} = i \left(\sum_{m \neq n} \frac{\langle u_m | \partial_{k_a} H | u_n \rangle \langle u_n | \partial_{k_b} H | u_m \rangle}{(E_m - E_n)^2} - (a \rightarrow b) \right). \quad (19)$$

It's convenient to rewrite the Hamiltonian in Eq. (16) with a pseudospin freedom σ :

$$H_1 = (3JS + P)\sigma_0 + \mathbf{h}(\mathbf{k}) \cdot \sigma + \mathbf{g}(\mathbf{k}) \cdot \sigma \quad (20)$$

where effective field vector \mathbf{h} is $(-(JS - Q)|\gamma_{\mathbf{k}}| \cos \phi_{\mathbf{k}}, (JS - Q)|\gamma_{\mathbf{k}}| \sin \phi_{\mathbf{k}}, -2DS\beta_{\mathbf{k}})$, $\sigma = (\sigma_x, \sigma_y, \sigma_z)$ is the Pauli matrix, and $\mathbf{g}(\mathbf{k}) = (-|g_{\mathbf{k}}| \cos \phi_{g_{\mathbf{k}}}, |g_{\mathbf{k}}| \sin \phi_{g_{\mathbf{k}}}, \delta_m)$. Within this representation, we put the band physics on a Bloch sphere, and all the geometric and topological properties are contained in the $\mathbf{h} \cdot \sigma + \mathbf{g} \cdot \sigma$ term. We plot the modified Berry curvature in Fig. 4(b), the xx and yy components of quantum metric G in Fig. 4(c)-(d). We can see that the QGT is renormalized to a new distribution in BZ by interaction-induced Zeeman field $g_{\mathbf{k}}$. The shifted Dirac points and the renormalized bands can be detected by well-established techniques including Brillouin light scattering, inelastic X-ray scattering, and inelastic neutron scattering [41–44].

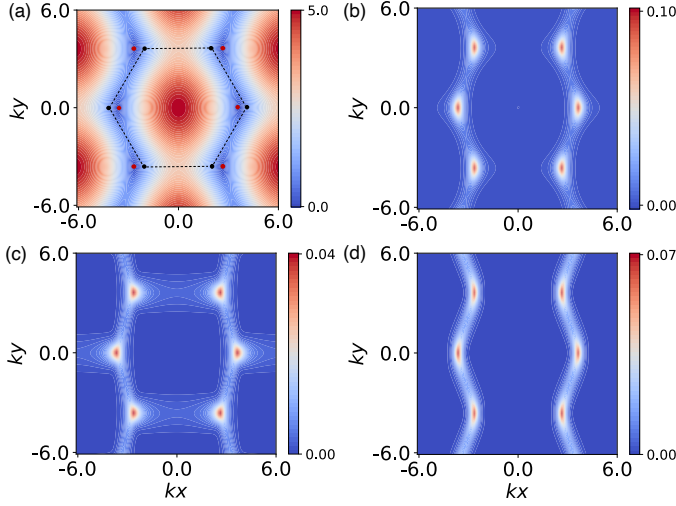


FIG. 4. Quantum geometric tensor in renormalised magnon bands. (a) The shift of Dirac points by anisotropic magnon amplification shown in Fig. 3(a) without DM interaction. Black dots represent the original Dirac points, and the shifted Dirac points are shown in red dots. (b) The distribution of Berry curvature shows the broken C_6 symmetry by interaction effect. (c) Quantum metric G_{xx} component. (d) Quantum metric G_{yy} component.

B. Topological bands with tunable Chern numbers

From Eq. (20), we find that interaction gives rise to an effective mass δ_m , which can be understood as an out-of-plane Zeeman field on the pseudospin degrees of freedom. The effective mass term determining the bandgap is essential for the geometric effect and the non-trivial band topology. The competition between the DM term $2DS\beta_k$ and δ_m can lead to the different Chern numbers and thus distinct topology. One should note that δ_m depends on DMI, as can be seen from the expression $\delta_m = \frac{JB}{2N_L} \sum_{\mathbf{k}_1} \Theta^+(\mathbf{k}_1)$, where the parameter $B \propto DS$. When $D = 0$, δ_m vanishes.

The total mass term is given by $m_H = 2DS\beta_k - \delta_m$. By tuning the magnon population, we can achieve topological phase transitions in the bottom band from $C = 1$ to $C = -1$ or $C = -1$ to $C = 1$. This is due to the fact that δ_m is dominated by the total population at point \mathbf{k}_1 , which can be driven by pumping magnons in both branches or by thermal excitation. Our results show that the total mass term decreases linearly with increasing magnon population, as illustrated in Fig. 5(a). The sign-change of m_H reveals a topological phase transition with reversing of the Chern numbers. A recent study has proposed a similar topological phase transition by the thermal excitation [45]. We argue that the band topology can be simply tuned using a magnon amplification approach, which will be discussed in Sec. V. The parametric amplification approach exhibits more advantages over the thermal excitation due to its flexibility [32].

By properly tuning the magnon population with the external EM field, we can increase the number of crossing points between the upper and lower magnon branches. This, in principle, can give rise to magnon bands with the higher Chern

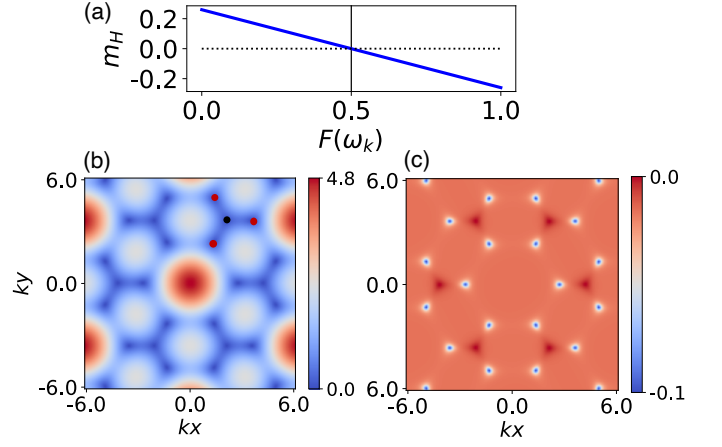


FIG. 5. Renormalized magnon bands with high Chern number, we use $D/J = 0.05$. (a). Renormalized Haldane mass at Dirac point in magnon bands we use $D/J = 0.05$, $F(\omega_k) = \frac{1}{4N_L} \sum_{\mathbf{k}_1} (f(\omega_{d_{\mathbf{k}_1}}) + f(\omega_{u_{\mathbf{k}_1}}))$ is the quantity for the normalised magnon density. (b) The energy difference $\Delta\omega_k/JS$ between upper and lower bands. The original Dirac point is labeled in black dot, and the three satellitic Dirac points are shown by red dots. (c) Berry curvature distributions.

numbers. Mathematically, the interaction-induced $g(\mathbf{k})$ can have any form. The general expression of $g(\mathbf{k})$ consists of a linear combination of the n -th nearest geometric factors $\gamma_{\mathbf{k}}^{(n)}$, or $g(\mathbf{k}) = \sum_n c_n \gamma_{\mathbf{k}}^{(n)}$, where $\gamma_{\mathbf{k}}^{(n)} = \sum_j e^{i\mathbf{k} \cdot \mathbf{r}_j^{(n)}}$, and $\mathbf{r}_j^{(n)}$ is the n -th nearest bond. As a specific example, let us look at the model of $g(\mathbf{k}) = c \sum_n e^{i\mathbf{k} \cdot \boldsymbol{\eta}_n}$, where c is expressed as the strength of the vector potential, and $\boldsymbol{\eta}_n$ is the geometric vector. We find that when $\boldsymbol{\eta}_n$ is for the third-nearest bonds, there are three more Dirac points at each \mathbf{K} valley as illustrated in Fig. 5(b). We introduce a nonzero DMI to gap all the Dirac points, and obtain the Berry curvature distribution of the lower band as shown in Fig. 5(c). In this case the Chern number of the lower magnon band is given by $C = \int_{BZ} \Omega_{\mathbf{k}} d\mathbf{k} = -2$.

C. Topological flat bands by parametric pumping

Using isotropic parametric pumping (see details in Sec. V A), we can engineer a topologically flat magnon band with a very small bandwidth. We employ Eq. (17) with pumped magnons that are located in a circle with equal energy as shown in Fig. 3(c). The energy of the pumped magnon is $\omega(\mathbf{k}) \approx 1.6J$, for $D/J = 0.1$, and the population intensity I_p is about 7.2. The resulting flat bands are shown in Fig. 6(a) by the solid curves. The flatness of the topological bands can be simply characterized by the ratio $r_f = \frac{w_p}{w_r}$, where w_p is the bandwidth without magnon-magnon interactions, and w_r is the bandwidth of the renormalized magnon spectrum. The computed value of $r_f \approx 0.09$ implies that the renormalized bands are almost dispersionless.

The almost flat topological bands give rise to a more uniform Berry curvature and quantum metric tensors that mimic

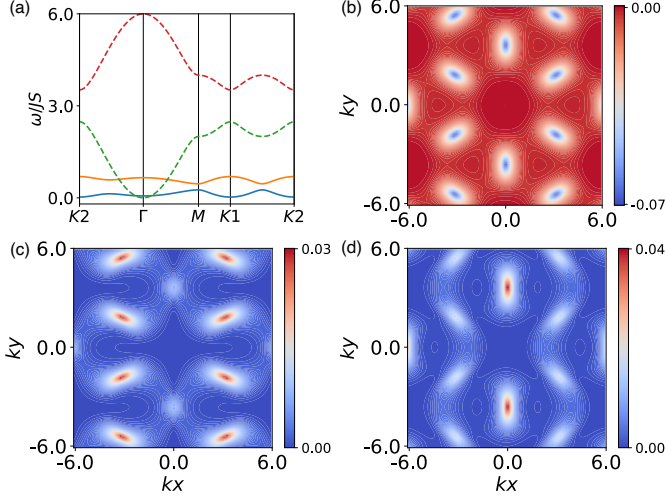


FIG. 6. QGT in topologically flat bands. (a) The topologically flat band by magnon-magnon interactions. Solid curves are interaction induced flat bands, and the dashed curves are noninteracting magnon bands. (b) The Berry curvature is redistributed by the interaction effect. (c) Quantum metric G_{xx} component. (d) Quantum metric G_{yy} component.

Landau level physics of interacting particles [46]. The quantum geometric properties are illustrated in Fig. 6(b)-(d). The Berry curvature is redistributed and the hotspots are shifted from K to M points in the BZ. The elements G_{xx} and G_{yy} of the quantum metric tensor in Fig. 6(c)-(d) are also strongly renormalized.

The renormalized magnon Bloch bands also conform to the ideal flat band condition that is provided by [47]:

$$\sqrt{\det G(\mathbf{k})} - \frac{1}{2} |\Omega(\mathbf{k})| = 0, \quad (21)$$

where $\det G(\mathbf{k}) = G_{xx}G_{yy} - G_{xy}G_{yx}$ is the determinant of quantum metric tensor. The nearly dispersionless magnon bands with ideal flat conditions allow us to investigate strongly correlated behaviour, since the interaction strength between the magnons is comparable to the bandwidth. Thus, we can expect the superfluid-Bose insulator transition at the partially filled lowest band [48]. More interestingly, the band minimum is also modified, which shifts from Γ point to K point, where there is a gapped Dirac cone with finite Berry curvatures and nonzero quantum metric. The induced flat band can potentially host a novel Bose-Einstein condensate that is stabilized by the nonzero quantum metric [49]. Furthermore, the emergent Goldstone modes from this flat band condensation reveal a quantum geometric dependency [50]. We argue that our interaction-induced flat magnon bands provide a realistic platform for studying this novel phenomenon, which deserves further theoretical study.

IV. SECOND ORDER RENORMALIZATION AND MAGNON SCATTERING

In the previous section, we employed a mean-field approximation of the term $[\psi_{\mathbf{k}}, H']$, and directly obtained the first-order self-energy. In order to include the higher-order renormalization, we must consider the dynamics of the commutator $[\psi_{\mathbf{k}}, H']$. The second-order effect from the quartic DM interactions is neglected, due to its smallness in the order of $\frac{D^2}{J^2}$. In this section, we focus on the second-order approximation by considering the equation of motion of retarded Green's function with the commutator $[\psi_{\mathbf{k}}, H']$:

$$\omega \langle [\psi_{\mathbf{k}}, H']; \psi_{\mathbf{k}'}^\dagger \rangle_\omega = \langle [[\psi_{\mathbf{k}}, H'], \psi_{\mathbf{k}'}^\dagger] \rangle + \langle [[\psi_{\mathbf{k}}, H'], H]; \psi_{\mathbf{k}'}^\dagger \rangle_\omega. \quad (22)$$

The second-order self-energy from perturbation theory can be written as:

$$\Sigma_{\mathbf{k}}^{(2)} = \frac{1}{2} \sum_{\{\mathbf{k}_i\}} \frac{V_{(\mathbf{k}_3, \mathbf{k}_4)}^{(\mathbf{k}, \mathbf{k}_2)} V_{(\mathbf{k}_2, \mathbf{k})}^{(\mathbf{k}_4, \mathbf{k}_3)} (n_{\mathbf{k}_2} (1 + n_{\mathbf{k}_3} + n_{\mathbf{k}_4}) - n_{\mathbf{k}_3} n_{\mathbf{k}_4})}{\omega_{\mathbf{k}} + i\varepsilon - \mathcal{M}(\mathbf{k}_2, \mathbf{k}_3, \mathbf{k}_4)}, \quad (23)$$

where $V_{(\mathbf{k}_3, \mathbf{k}_4)}^{(\mathbf{k}, \mathbf{k}_2)} = V_{\mathbf{k}_3, \mathbf{k}_4}^{\mathbf{k}, \mathbf{k}_2} + V_{\mathbf{k}_3, \mathbf{k}_4}^{\mathbf{k}_2, \mathbf{k}} + V_{\mathbf{k}_4, \mathbf{k}_3}^{\mathbf{k}, \mathbf{k}_2} + V_{\mathbf{k}_4, \mathbf{k}_3}^{\mathbf{k}_2, \mathbf{k}}$ is the interacting coefficient matrix. The nonzero matrix elements from the interacting Hamiltonian are $V_{1,2}^{1,2} = -\frac{J}{4N_L} \gamma_{\mathbf{k}_4 - \mathbf{k}_2}$, $V_{2,2}^{1,2} = \frac{J}{4N_L} \gamma_{\mathbf{k}_1}$, $V_{1,1}^{2,1} = \frac{J}{4N_L} \gamma_{\mathbf{k}_1}^*$, $V_{2,1}^{2,2} = \frac{J}{4N_L} \gamma_{\mathbf{k}_4}^*$ and $V_{1,2}^{1,1} = \frac{J}{4N_L} \gamma_{\mathbf{k}_4}$. We define $V_{c,d}^{a,b} \triangleq V_{c\mathbf{k}_3, d\mathbf{k}_4}^{a\mathbf{k}_1, b\mathbf{k}_2}$, and $a, b, c, d \in \{1, 2\}$ are the labels for the two components of spinor $\psi_{\mathbf{k}} (\psi_{\mathbf{k}}^\dagger)$. The function $n_{\mathbf{k}}$ denotes the zeroth order population matrix $\langle \psi_{\mathbf{k}}^\dagger \psi_{\mathbf{k}} \rangle^{(0)}$, which can be the equilibrium or non-equilibrium distribution function. $\mathcal{M}(\mathbf{k}_2, \mathbf{k}_3, \mathbf{k}_4)$ is a tensor dominated by the elements of $M(\mathbf{k}_2)$, $M(\mathbf{k}_3)$ and $M(\mathbf{k}_4)$. The definition of $\mathcal{M}(\mathbf{k}_2, \mathbf{k}_3, \mathbf{k}_4)$ comes from the operation:

$$\begin{aligned} \mathcal{M} \psi_{\mathbf{k}_2}^\dagger \psi_{\mathbf{k}_3} \psi_{\mathbf{k}_4} &= \psi_{\mathbf{k}_2}^\dagger M(\mathbf{k}_3) \psi_{\mathbf{k}_3} \psi_{\mathbf{k}_4} + \psi_{\mathbf{k}_2}^\dagger \psi_{\mathbf{k}_3} M(\mathbf{k}_4) \psi_{\mathbf{k}_4} \\ &\quad - \psi_{\mathbf{k}_2}^\dagger M(\mathbf{k}_2) \psi_{\mathbf{k}_3} \psi_{\mathbf{k}_4} \end{aligned} \quad (24)$$

We simplify this operation and obtain $Q'_{a,b,c}(\mathbf{k}_2, \mathbf{k}_3, \mathbf{k}_4) = \sum_{d,e,f} \mathcal{M}_{d,e,f}^{a,b,c}(\mathbf{k}_2, \mathbf{k}_3, \mathbf{k}_4) Q_{d,e,f}(\mathbf{k}_2, \mathbf{k}_3, \mathbf{k}_4)$, where $Q'_{a,b,c}$ is the element in RHS of above equation, $Q_{a,b,c}$ is the element in $\psi_{\mathbf{k}_2}^\dagger \psi_{\mathbf{k}_3} \psi_{\mathbf{k}_4}$. Since $\psi_{\mathbf{k}_2}^\dagger \psi_{\mathbf{k}_3} \psi_{\mathbf{k}_4}$ has 8 elements, it gives rise to $2^6 = 64$ elements in \mathcal{M} . Here we list the 8 diagonal elements of \mathcal{M} :

$$\begin{aligned} \mathcal{M}_{111}^{111} &= -M^{11}(\mathbf{k}_2) + M^{11}(\mathbf{k}_3) + M^{11}(\mathbf{k}_4), \\ \mathcal{M}_{222}^{222} &= -M^{22}(\mathbf{k}_2) + M^{22}(\mathbf{k}_3) + M^{22}(\mathbf{k}_4), \\ \mathcal{M}_{112}^{112} &= -M^{11}(\mathbf{k}_2) + M^{11}(\mathbf{k}_3) + M^{22}(\mathbf{k}_4), \\ \mathcal{M}_{121}^{121} &= -M^{11}(\mathbf{k}_2) + M^{22}(\mathbf{k}_3) + M^{11}(\mathbf{k}_4), \\ \mathcal{M}_{122}^{122} &= -M^{11}(\mathbf{k}_2) + M^{22}(\mathbf{k}_3) + M^{22}(\mathbf{k}_4), \\ \mathcal{M}_{211}^{211} &= -M^{22}(\mathbf{k}_2) + M^{11}(\mathbf{k}_3) + M^{11}(\mathbf{k}_4), \\ \mathcal{M}_{212}^{212} &= -M^{22}(\mathbf{k}_2) + M^{11}(\mathbf{k}_3) + M^{22}(\mathbf{k}_4), \\ \mathcal{M}_{221}^{221} &= -M^{22}(\mathbf{k}_2) + M^{22}(\mathbf{k}_3) + M^{11}(\mathbf{k}_4). \end{aligned} \quad (25)$$

These diagonal elements are the most important terms for determining the magnon-magnon scattering channels. It is more convenient to work with the self-energy matrix in an eigenmode basis, and transform the $\begin{pmatrix} a_{\mathbf{k}} \\ b_{\mathbf{k}} \end{pmatrix}$ basis to the eigenmode basis $\begin{pmatrix} d_{\mathbf{k}} \\ u_{\mathbf{k}} \end{pmatrix}$ using a unitary transformation U , where $d_{\mathbf{k}}(u_{\mathbf{k}})$ is the magnon operator for the lower (upper) band. As a consequence, \mathcal{M} has only diagonal components, and M is a diagonal matrix of the eigenvalues. Thus we have the second-order self-energy matrix in the eigenmode basis:

$$\tilde{\Sigma}_{\mathbf{k}}^{(2)} = \frac{1}{2} \sum_{\{k_i\}} \frac{\tilde{V}_{(k_3, k_4)}^{(k, k_2)} \tilde{V}_{(k_2, k)}^{(k_4, k_3)} (\tilde{n}_{k_2} (1 + \tilde{n}_{k_3} + \tilde{n}_{k_4}) - \tilde{n}_{k_3} \tilde{n}_{k_4})}{\omega_{\mathbf{k}} + i\varepsilon + \omega_{k_2} - \omega_{k_3} - \omega_{k_4}} \quad (26)$$

where $\tilde{V}_{(k_3, k_4)}^{(k, k_2)} = U_{\mathbf{k}}^\dagger U_{k_2}^\dagger V_{(k_3, k_4)}^{(k, k_2)} U_{k_3} U_{k_4}$ (see details in Appendix D). The expression of unitary U is given by:

$$\begin{pmatrix} a_{\mathbf{k}} \\ b_{\mathbf{k}} \end{pmatrix} = \frac{1}{\sqrt{2}} \begin{pmatrix} \sqrt{1 + \frac{B}{A}} e^{i\frac{\phi_{\mathbf{k}}}{2}} & \sqrt{1 - \frac{B}{A}} e^{i\frac{\phi_{\mathbf{k}}}{2}} \\ \sqrt{1 - \frac{B}{A}} e^{-i\frac{\phi_{\mathbf{k}}}{2}} & -\sqrt{1 + \frac{B}{A}} e^{-i\frac{\phi_{\mathbf{k}}}{2}} \end{pmatrix} \begin{pmatrix} d_{\mathbf{k}} \\ u_{\mathbf{k}} \end{pmatrix} \quad (27)$$

where A and B factors are given in Eq. (14), which are dominated by DM interactions. With the unitary transformations, we have all the interaction matrix elements on an eigenmode basis (see details in Appendix D).

The second-order self-energy term has a more complicated form, which not only modifies the bandwidth, but also leads to magnon damping. Replacing ω by $\omega_{\mathbf{k}} + i\varepsilon$ in Eq. (26), where the infinitesimal imaginary part $i\varepsilon$ is the argument of the retarded Green's function, we have $\tilde{\Sigma}_{\mathbf{k}}^{(2)} = \tilde{\Sigma}_{\mathbf{k}}^{(2)'} - i\tilde{\Sigma}_{\mathbf{k}}^{(2)''}$, where the real part is the renormalization term and the imaginary part is the damping term or magnon-magnon scattering rate [29]. The scattering rate contributes to the broadening of the magnon band, which gives rise to an upper bound of the magnon lifetime $\tau = \frac{\hbar}{2\tilde{\Sigma}_{\mathbf{k}}^{(2)''}}$.

We define the spectral function $A(\mathbf{k}, \omega)$, which describes quasiparticle properties in magnon spectrum (band information) and density of states. Essentially, $A(\mathbf{k}, \omega)$ is the imaginary part of the retarded Green's function:

$$A(\mathbf{k}, \omega) = -\frac{1}{\pi} \text{Im}(G_R(\mathbf{k}, \omega)) \quad (28)$$

The renormalized magnon dispersion at temperature $T/J = 0.5$ with the second-order self-energy is shown in Fig. 7(a). The blurred areas indicate the magnon damping effect from the imaginary component $\tilde{\Sigma}_{\mathbf{k}}^{(2)''}$. We compare the scattering rate of the two cases with and without DMI. One can see that DMI strongly influences the scattering rate, and the effect is momentum dependent, as shown in Fig. 7(b)-(d) – while the rate is enhanced at the K -point, it is suppressed at the M -point. We now focus on the scattering rate in the lower band. The rate near the Dirac point with DMI is significantly enhanced for the lower band, as shown in Fig. 7(c), indicating that the

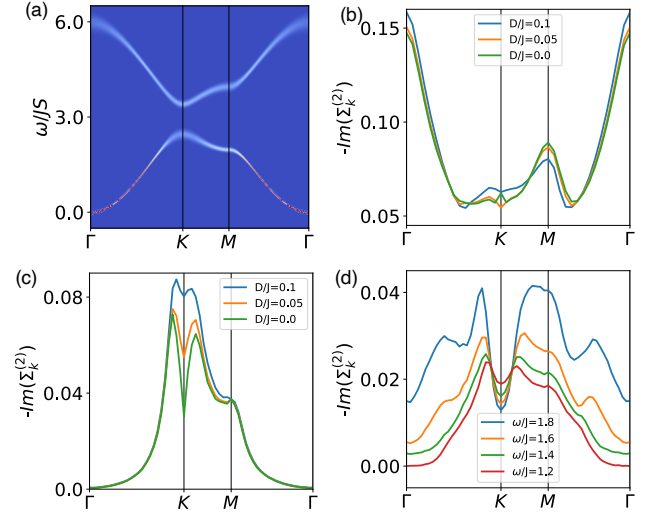


FIG. 7. Second-order renormalization of magnon dispersion, we use parameter $T/J=0.5$, and $D/J = 0.1$. (a) Spectral function $A(\mathbf{k}, \omega_{\mathbf{k}})$. In the plot, we use 1/10 of the maximal $A(\mathbf{k}, \omega_{\mathbf{k}})$ for the color mapping to make a better display of damping components. (b)-(c) The magnon scattering rates with different DMI. One pronounced feature is that DMI significantly enhances the scattering rate around Dirac point of the lower band, and gives rise to a faster decay dynamics. (d) Scattering rate in lower band by the magnon parametric amplifications. We here employ a very small temperature $T/J = 0.1$ to purely show the scattering effect from non-equilibrium magnon population.

DMI facilitates scattering rate and results in faster magnon dynamics. The simple explanation for the DMI-enhanced scattering rate at the Dirac point is that the nonzero topological gap contributes to a finite density of states for the Dirac magnon, and thus provides more scattering channels for interacting magnons.

We also study the scattering effect from the magnon parametric amplification, which can dramatically modify the scattering rate by changing the energy position of the amplified magnons; the basic features are shown in Fig. 7 (d). With a fixed magnon population intensity I_p , we increase the energy position from $\omega_{d_{\mathbf{k}}} = 1.2J$ to $1.8J$ for magnons out of equilibrium. The scattering rate along the k -points is increased except for the Dirac points. There are pronounced peaks between Γ and M points, which is due to the obvious scattering around the pumped magnons. We employ a very small temperature of $T/J = 0.1$ in the calculation to focus on the scattering effect from non-equilibrium magnon populations illustrating that the scattering rate can be flexibly tuned by the light-induced magnons. Magnon scattering rates are closely linked to the microscopic dynamics aspects, which provide powerful tools for measuring and controlling the magnetic order in the ultrafast time regime. This is a rapidly developing research area that is relevant for magnetic memory and spintronics [51].

V. PARAMETRIC AMPLIFICATIONS AND THERMAL HALL EFFECT

A. Parametric magnon amplifications

As we mentioned in previous sections, we can populate magnon by an external electromagnetic field [52], in addition to thermal excitations. The magnon population can be significantly enhanced by the so-called parametric instability while preserving the magnetic order in bulk state [32]. This instability can be induced by coupling the magnetic material to the external field, whereby excited magnons are created in pairs. Here we employ a coherent driving electromagnetic (EM) field and start with the effective coupling Hamiltonian:

$$H_{int} = \sum_{\mathbf{k}} \frac{g_{\mathbf{k}}}{2} (d_{-\mathbf{k}}^\dagger d_{\mathbf{k}}^\dagger b + b^\dagger d_{\mathbf{k}} d_{-\mathbf{k}}), \quad (29)$$

where the field operator $b \approx \beta \exp(-i\Omega_0 t)$ is the external EM field or the pump photon, and $g_{\mathbf{k}} \approx g$ is the coupling coefficient between external field and magnon excitation that can be treated as momentum independent in a small bandwidth regime. H_{int} describes the process of creation of a pair of magnons by absorption of a photon (and, by hermiticity of the coupling Hamiltonian, the reverse process of annihilation of a pair of magnons accompanied by the emission of a photon). Magnons need to be created (or annihilated) in pairs with equal and opposite momenta to satisfy the conservation of momentum during the process (photons carry zero momentum). For the single-particle Hamiltonian, we have to include the scattering terms H_{imp} caused by impurities and disorders. The magnon density is determined by the time-dependent Heisenberg equation of motion as follows [32]:

$$i \frac{dT_{\mathbf{k}}(t)}{dt} = \langle [\hat{T}_{\mathbf{k}}, H] \rangle = \tilde{\Omega}_{\mathbf{k}} T_{\mathbf{k}}(t), \quad H = H_1 + H_{int} + H_{imp}, \quad (30)$$

where operator $\hat{T}_{\mathbf{k}}(t) = (d_{\mathbf{k}}, d_{-\mathbf{k}}^\dagger)$, and $T_{\mathbf{k}}(t) = (\langle d_{\mathbf{k}} \rangle, \langle d_{-\mathbf{k}}^\dagger \rangle)$ are the classical amplitudes of the magnon fields, and $\tilde{\Omega}_{\mathbf{k}}$ is the dynamical matrix, which has the eigenvalues:

$$\omega_{\mathbf{k}, \pm} = \frac{\omega_{\mathbf{k}} - \omega_{-\mathbf{k}}}{2} - \frac{i\gamma}{2} \pm \sqrt{\frac{(\omega_{\mathbf{k}} + \omega_{-\mathbf{k}} - \Omega_0)^2}{2} - \varepsilon^2}, \quad (31)$$

where γ denotes a linear dissipative damping, which is dominated by H_{imp} , and $\varepsilon = g\beta$ is the overall coupling strength. When the detuning term $\omega_{\mathbf{k}} + \omega_{-\mathbf{k}} - \Omega_0 \approx 0$, the imaginary part of $\omega_{\mathbf{k}, \pm}$ becomes $\varepsilon - \gamma/2$, and the magnon density at \mathbf{k} is $\langle d_{\mathbf{k}} \rangle \propto e^{(\varepsilon - \gamma/2)t}$. When the coupling strength ε exceeds the dissipation γ , there is an exponential growth of the magnon density in mode \mathbf{k} , and resonant amplification is achieved. This limits the growth in amplified magnon density can be modelled by a phenomenological nonlinear damping constant η . Thus, the dynamical equation of magnon population $\langle d_{\mathbf{k}} \rangle$ is given by:

$$i \frac{dI_p}{dt} = \left(\tilde{\omega}_{\mathbf{k}} - \tilde{\omega}_{-\mathbf{k}} - i(\gamma + \eta I_p) + i\sqrt{4\varepsilon^2 - (\tilde{\omega}_{\mathbf{k}} + \tilde{\omega}_{-\mathbf{k}})^2} \right) I_p, \quad (32)$$

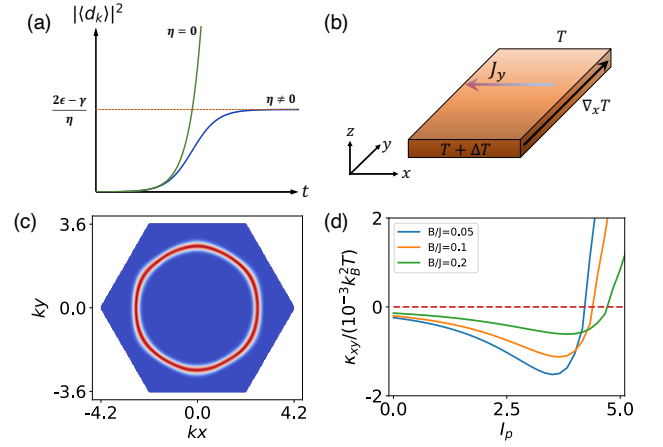


FIG. 8. Thermal Hall effect with parametric amplifications (a) Magnon intensity is a function of parametric amplifications. (b) The schematic plot for thermal Hall measurements. (c) The position of amplified magnon in Brillouin zone. (d) The thermal Hall conductivity with different magnetic fields. We set $T/J = 0.2$ in the calculations.

where $I_p = |\langle d_{\mathbf{k}} \rangle|^2$ is the magnon population intensity. When the resonance condition $\omega_{\mathbf{k}} + \omega_{-\mathbf{k}} = \Omega_0$ is reached, we can easily solve the dynamical equation and obtain the typical solution as:

$$I_p = \frac{1}{\frac{\eta}{2\varepsilon - \gamma} + c_0 e^{-2(\varepsilon - \gamma)t}}. \quad (33)$$

When $t \rightarrow \infty$, we have the steady-state magnon intensity $I_p = \frac{2\varepsilon - \gamma}{\eta}$, which is determined by the magnon-photon coupling strength and the dissipation coefficients γ and η . The amplification dynamics is shown in Fig. 8(a). Thus, we can employ the amplification scheme to populate the magnon at specific momenta in the BZ, which will give rise to a tunable many-body effect on magnon quasiparticles and transport properties.

B. Thermal Hall effect for Dirac magnon

One direct application of the parametric amplification is the modification of the magnon thermal Hall effect and the use of this effect as an experimental tool for probing the topological character of the magnon bands and their renormalization due to interaction effects. The schematic plot of thermal Hall measurement is shown in Fig. 8(b). With the thermal gradient along the x-direction, one can measure the thermal Hall conductance along the y-direction. The calculation of the thermal conductivity κ^{xy} in a slab geometry yields [13, 53, 54]:

$$\kappa^{xy} = -\frac{k_B^2 T}{(2\pi)^2} \sum_n \int d^2 \mathbf{k} c_2(f(\omega_n(\mathbf{k}))) \Omega_n^{xy}(\mathbf{k}), \quad (34)$$

where k_B is Boltzmann constant, $f(\omega_n(\mathbf{k}))$ is the magnon density distribution that, in the present case, has contributions from both thermally excited magnons – whose population is given by the Bose-Einstein (BE) distribution function,

$f(\omega_n(\mathbf{k})) = \frac{1}{e^{\omega_n(\mathbf{k})\beta} - 1}$ – as well as those generated by EM radiation. The function $c_2(u)$ is given by [54]:

$$c_2(u) = (1+u) \left[\ln \left(1 + \frac{1}{u} \right) \right]^2 - [\ln(u)]^2 - 2\text{Li}_2(-u), \quad (35)$$

with $\text{Li}_2(u) = \sum_{k=1}^{\infty} \frac{u^k}{k^2}$ as the polylogarithm function, and $\Omega_n^{xy}(\mathbf{k})$ is the Berry curvature of n -th band.

In thermal Hall transport with the magnon amplifications, the interaction between the thermally generated magnons and light-induced magnons is delicate. To fully solve this transport problem, we need to employ a self-consistent solution. However, this is beyond the scope of this paper. For simplicity, we consider the system at low temperature, so that the band renormalization effect from thermally excited magnons is negligible. Furthermore, we ignore the second-order scattering processes from magnon-magnon interactions in the transport measurement due to the low temperature.

With these simplifications, we focus on the thermal transport in the mean-field renormalized band by amplified magnons. We apply a monochromatic external EM field with energy $\Omega_0 = 3.2J$ that can only produce magnon populations at the energy $\omega_{\mathbf{k}} = \frac{\Omega_0}{2}$ in the lower band, as shown in Fig. 8 (c). The advantage of this scheme is that the amplified magnons with the energy $\Omega_0 = 1.6J$ do not contribute to the thermal Hall signal due to the zero Berry curvature at their locations, thus we can only have the thermal Hall response from the thermally excited magnons. We use the magnon intensity I_p as the controllable variable, and the calculated thermal Hall conductivity is shown in Fig. 8(d). One can see that each curve has a transition point I_p^c where the thermal Hall signal is going to reverse the signs. This originates from the topological phase transitions that are discussed in Sec. III B. The thermal Hall signals change the sign when the Chern number of the magnon band is reversed. An increase in the thermal Hall signal is expected to occur before the transition point due to the reduction of the bandwidth. When I_p is close to the transition point, the topological gap is closed, thus the signal becomes zero. The thermal Hall signal sharply increases after the reopening of the topological gap.

We also show that the transition points are magnetic field-dependent. The increase of the magnetic field gives rise to a larger critical point I_p^c as shown in Fig. 8(d). Thus with a larger magnetic field, one may need a higher magnon intensity to achieve the topological phase transition. Therefore the thermal Hall measurement can be a useful experimental tool for exploring the interaction-induced topological phase transition.

VI. CONCLUSIONS

To summarize, we show much interesting physics arises from the magnon systems with non-trivial DM interaction, when the effect of magnon-magnon interaction is properly accounted for. Our perturbative calculation shows the possibility of magnon band engineering exploiting such interaction, especially when the magnon density can be flexibly induced in

different parts of the BZ with parametric amplification by the electromagnetic field. Such band engineering allows us to experimentally tune the bandwidth and the Berry curvature distribution. With properly designed amplification schemes, we can even induce band inversions leading to topological phase transitions. The transport properties of magnons under either a magnetic field gradient or a thermal gradient are very sensitive to the geometric and topological properties of the band. This allows us to propose a number of scenarios to experimentally probe the interplay between geometry, topology, and many-body effects in magnon systems.

The interaction-induced reduction of bandwidth and shift of the Dirac points can be detected by well-established techniques including Brillouin light scattering, inelastic X-ray scattering, and inelastic neutron scattering. By combining the computed quantum geometric tensor and the interaction-induced Haldane mass term, the thermal Hall conductivity of the magnons provides a direct diagnosis of the geometric and topological properties of the magnonic Chern bands by the external pumping field. More importantly, we can achieve flat bands with non-trivial topology, that provides a realistic platform for the study of strongly correlated bosonic systems such as superfluid-insulator transitions and flat band Bose-Einstein condensation.

By applying a second-order perturbation theory, we also reveal that the magnon scattering rate is significantly enhanced near the Dirac point with the DMI, which has not been studied before. Such scattering from magnon-magnon interaction can play an important role in the stability of the Dirac magnons and their decay dynamics. This is especially the case for systems with the intrinsic large interaction and small bandwidth, and our study highlights that the magnonic Dirac materials could serve as useful platforms for many-body physics arising from lattice bosons with non-trivial band topologies.

ACKNOWLEDGMENTS

B.Y. would like to acknowledge the support from the Singapore National Research Foundation (NRF) under NRF fellowship award NRF-NRFF12-2020-0005, and a Nanyang Technological University start-up grant (NTU-SUG). P.S. acknowledges financial support from the Ministry of Education, Singapore through MOE2019-T2-2-119.

Appendix A: Effective tight-binding model of magnon by Holstein-Primakov transformation

Generally, by HP transformation, the spin operators can be expressed as the nonlinear functions of magnon operators:

$$S_i^+ = \sqrt{2S} \sqrt{1 - \frac{a_i^\dagger a_i}{2S}} a_i, \quad S_i^- = \sqrt{2S} a_i^\dagger \sqrt{1 - \frac{a_i^\dagger a_i}{2S}} \quad (\text{A1})$$

Up to the first-order Taylor expansion, we have:

$$S_i^+ = \sqrt{2S} \left(a_i - \frac{a_i^\dagger a_i a_i}{4S} \right), \quad S_i^- = \sqrt{2S} \left(a_i^\dagger - \frac{a_i^\dagger a_i^\dagger a_i}{4S} \right) \quad (\text{A2})$$

$$\begin{aligned} \sum_{\alpha\beta\gamma} \varepsilon_{\alpha\beta\gamma} v_{ij}^\alpha S_i^\beta S_j^\gamma &= v_{ij}^\alpha \left(S_i^\alpha S_j^\alpha - S_i^\alpha S_j^\alpha \right) \\ &= i v_{ij}^\alpha \frac{S}{2} \left(a_i^\dagger + a_i - \frac{a_i^\dagger a_i a_i + a_i^\dagger a_i^\dagger a_i}{4S} \right) \left(a_j^\dagger - a_j - \frac{a_j^\dagger a_j^\dagger a_j - a_j^\dagger a_j a_j}{4S} \right) - i v_{ij}^\alpha \frac{S}{2} \left(a_i^\dagger - a_i - \frac{a_i^\dagger a_i^\dagger a_i - a_i^\dagger a_i a_i}{4S} \right) \left(a_j^\dagger + a_j - \frac{a_j^\dagger a_j a_j + a_j^\dagger a_j^\dagger a_j}{4S} \right) \\ &= -i v_{ij}^\alpha S a_i^\dagger a_j + H.c. + \boxed{i \frac{v_{ij}^\alpha}{4} a_i^\dagger a_i^\dagger a_i a_j + i \frac{v_{ij}^\alpha}{4} a_i^\dagger a_j^\dagger a_j a_j + H.c.}. \end{aligned} \quad (\text{A4})$$

The terms in the box are quartic DM interactions, which are very important for the topological phase transitions. The quartic DM interactions in k-space are written as:

$$H'_{DM} = \sum_{\mathbf{k}_i} D_{\mathbf{k}_3, \mathbf{k}_4}^{\mathbf{k}_1, \mathbf{k}_2} \left(a_{\mathbf{k}_1}^\dagger a_{\mathbf{k}_2}^\dagger a_{\mathbf{k}_3} a_{\mathbf{k}_4} - b_{\mathbf{k}_1}^\dagger b_{\mathbf{k}_2}^\dagger b_{\mathbf{k}_3} b_{\mathbf{k}_4} \right), \quad (\text{A5})$$

where $D_{\mathbf{k}_3, \mathbf{k}_4}^{\mathbf{k}_1, \mathbf{k}_2} = \frac{D}{2N_L} (\beta_{\mathbf{k}_4} + \beta_{\mathbf{k}_1})$.

If there is a NNN spin coupling, we then have the following spin Hamiltonian:

$$H_{nnn} = \sum_{i,j} J' S_i \cdot S_j, \quad (\text{A6})$$

where J' is the next nearest neighbour exchange parameter. Using HP transformation, we have the effective tight-binding model, which is written as:

$$\begin{aligned} H_{nnn} &= J' S \sum_{\langle i,j \rangle} (a_i a_j^\dagger + a_i^\dagger a_j) + \\ &\frac{J'}{4} \sum_{\langle i,j \rangle} (4a_i^\dagger a_i a_j^\dagger a_j - a_i^\dagger a_j^\dagger a_j a_j - a_j^\dagger a_j^\dagger a_i a_j - a_i^\dagger a_j^\dagger a_i a_i - a_i^\dagger a_i^\dagger a_i a_j). \end{aligned} \quad (\text{A7})$$

The first term in RHS is the NNN single-particle term. Employing the Fourier transformation, we have the interacting Hamiltonian in k-space:

$$H'_{nnn} = \sum_{\mathbf{k}_i} G_{\mathbf{k}_3, \mathbf{k}_4}^{\mathbf{k}_1, \mathbf{k}_2} \left(a_{\mathbf{k}_1}^\dagger a_{\mathbf{k}_2}^\dagger a_{\mathbf{k}_3} a_{\mathbf{k}_4} + b_{\mathbf{k}_1}^\dagger b_{\mathbf{k}_2}^\dagger b_{\mathbf{k}_3} b_{\mathbf{k}_4} \right). \quad (\text{A8})$$

where the $G_{\mathbf{k}_3, \mathbf{k}_4}^{\mathbf{k}_1, \mathbf{k}_2} = \frac{J'}{2N_L} (2 - \sum_n \text{Re}(e^{i\mathbf{k}_1 \cdot \sigma_n}) - \sum_n \text{Re}(e^{i\mathbf{k}_4 \cdot \sigma_n}))$ is the interaction coefficient.

Then we have the Hamiltonian with magnon-magnon interaction terms:

$$\begin{aligned} H &= \left(-JS \sum_{ij} a_i^\dagger a_j + h.c. \right) + 3JS \sum_i a_i^\dagger a_i - 3N_L JS^2 - J \sum_{ij} a_i^\dagger a_i a_j^\dagger a_j \\ &\quad + \frac{J}{4} \sum_{ij} \left(a_i^\dagger a_j^\dagger a_j a_i + a_j^\dagger a_j^\dagger a_i a_j + a_i^\dagger a_j^\dagger a_i a_i + a_i^\dagger a_i^\dagger a_i a_j \right). \end{aligned} \quad (\text{A3})$$

Further, we have:

Appendix B: First-order renormalization of magnon band

In this section we give a detailed derivation of the first order renormalization. We follow Zubarev and employ the retarded Green's function formalism:

$$\begin{aligned} \langle \Psi(\mathbf{r}, t); \Psi^\dagger(\mathbf{r}', t') \rangle &= -i\theta(t-t') \langle [\Psi(\mathbf{r}, t), \Psi^\dagger(\mathbf{r}', t')] \rangle \\ &= -i\theta(t-t') (\langle \Psi(\mathbf{r}, t) \Psi^\dagger(\mathbf{r}', t') \rangle - \langle \Psi^\dagger(\mathbf{r}', t') \Psi(\mathbf{r}, t) \rangle) \end{aligned} \quad (\text{B1})$$

where $\theta(t-t')$ is the step function, and $\Psi^\dagger(\mathbf{r}, t)$ is the field operator of spinor which can be written as $(\sum_i \phi_{a,i}^*(\mathbf{r}) a_i^\dagger(t), \sum_i \phi_{b,i}^*(\mathbf{r}) b_i^\dagger(t))$, where $a_i^\dagger(t)$ and $b_i^\dagger(t)$ are the magnon creation operators of (A, B)-site in bipartite honeycomb lattice. The equation of motion for retarded Green's function is:

$$\begin{aligned} i \frac{\partial}{\partial t} \langle \Psi(\mathbf{r}, t); \Psi^\dagger(\mathbf{r}', t') \rangle &= \delta(\mathbf{r} - \mathbf{r}') \delta(t - t') + \langle [\Psi(\mathbf{r}, t), H(t)]; \Psi^\dagger(\mathbf{r}', t') \rangle \end{aligned} \quad (\text{B2})$$

Using Fourier transformation, we study the above dynamical equation in the frequency domain and k-space. Then we have:

$$\begin{aligned} \omega \langle \Psi_{\mathbf{k}}; \Psi_{\mathbf{k}'}^\dagger \rangle_\omega &= \langle [\Psi_{\mathbf{k}}, \Psi_{\mathbf{k}'}^\dagger] \rangle + \langle [\Psi_{\mathbf{k}}, H]; \Psi_{\mathbf{k}'}^\dagger \rangle_\omega \\ &= \langle [\Psi_{\mathbf{k}}, \Psi_{\mathbf{k}'}^\dagger] \rangle + \langle [\Psi_{\mathbf{k}}, H_0]; \Psi_{\mathbf{k}'}^\dagger \rangle_\omega + \langle [\Psi_{\mathbf{k}}, H']; \Psi_{\mathbf{k}'}^\dagger \rangle_\omega. \end{aligned} \quad (\text{B3})$$

Fist we check the zero-order Green's function with $H = H_0$, which is for the noninteracting magnon particle:

$$\omega \langle \psi_{\mathbf{k}}; \psi_{\mathbf{k}'}^\dagger \rangle_\omega = \delta_{\mathbf{k}, \mathbf{k}'} + \langle [\psi_{\mathbf{k}}, H_0]; \psi_{\mathbf{k}'}^\dagger \rangle_\omega:$$

$$\langle \psi_{\mathbf{k}}; \psi_{\mathbf{k}'}^\dagger \rangle_\omega^0 = \frac{\delta_{\mathbf{k}, \mathbf{k}'}}{\omega - M_{\mathbf{k}}} \quad (\text{B4})$$

where $[\psi_{\mathbf{k}}, H_0] = [\psi_{\mathbf{k}}, \sum_{\mathbf{k}''} \psi_{\mathbf{k}''}^\dagger M_{\mathbf{k}''} \psi_{\mathbf{k}''}] = M_{\mathbf{k}} \psi_{\mathbf{k}}$. The equation of motion of Green's function now reads:

$$\langle \psi_{\mathbf{k}}; \psi_{\mathbf{k}'}^\dagger \rangle_\omega = \frac{\langle [\psi_{\mathbf{k}}, \psi_{\mathbf{k}'}^\dagger] \rangle}{\omega - M(\mathbf{k})} + (\omega - M(\mathbf{k}))^{-1} \langle [\psi_{\mathbf{k}}, H']; \psi_{\mathbf{k}'}^\dagger \rangle_\omega$$

$$= \langle \psi_{\mathbf{k}}; \psi_{\mathbf{k}'}^\dagger \rangle_\omega^0 + \langle \psi_{\mathbf{k}}; \psi_{\mathbf{k}'}^\dagger \rangle_\omega^0 \langle [\psi_{\mathbf{k}}, H']; \psi_{\mathbf{k}'}^\dagger \rangle_\omega. \quad (\text{B5})$$

The poles of Green's function give rise to the 2×2 noninteracting magnon bands. We can have a general interaction terms with the form: $H' = \sum_{\{\mathbf{k}_i\}} V_{\mathbf{k}_3, \mathbf{k}_4}^{k_1, k_2} \psi_{\mathbf{k}_1}^\dagger \psi_{\mathbf{k}_2}^\dagger \psi_{\mathbf{k}_3} \psi_{\mathbf{k}_4}$. Each wave vector index in interaction matrix element has two components due to the spinor property of $\psi_{\mathbf{k}}^\dagger$:

$$\sum_{\mathbf{k}_1, \mathbf{k}_3} V_{\mathbf{k}_3, \mathbf{k}_4}^{k_1, k_2} \psi_{\mathbf{k}_1}^\dagger \psi_{\mathbf{k}_3} = \sum_{\mathbf{k}_1, \mathbf{k}_3} V_{1\mathbf{k}_3, \mathbf{k}_4}^{1k_1, k_2} a_{\mathbf{k}_1}^\dagger a_{\mathbf{k}_3} + \sum_{\mathbf{k}_1, \mathbf{k}_3} V_{2\mathbf{k}_3, \mathbf{k}_4}^{1k_1, k_2} a_{\mathbf{k}_1}^\dagger b_{\mathbf{k}_3}$$

$$+ \sum_{\mathbf{k}_1, \mathbf{k}_3} V_{1\mathbf{k}_3, \mathbf{k}_4}^{2k_1, k_2} b_{\mathbf{k}_1}^\dagger a_{\mathbf{k}_3} + \sum_{\mathbf{k}_1, \mathbf{k}_3} V_{2\mathbf{k}_3, \mathbf{k}_4}^{2k_1, k_2} b_{\mathbf{k}_1}^\dagger b_{\mathbf{k}_3} \quad (\text{B6})$$

We have the commutator term:

$$[\psi_{\mathbf{k}}, H'] = \sum_{\{\mathbf{k}_i\}} V_{\mathbf{k}_3, \mathbf{k}_4}^{k_1, k_2} [\psi_{\mathbf{k}}, \psi_{\mathbf{k}_1}^\dagger \psi_{\mathbf{k}_2}^\dagger \psi_{\mathbf{k}_3} \psi_{\mathbf{k}_4}]$$

$$= \sum_{\{\mathbf{k}_i\}} V_{\mathbf{k}_3, \mathbf{k}_4}^{(k, k_2)} \psi_{\mathbf{k}_2}^\dagger \psi_{\mathbf{k}_3} \psi_{\mathbf{k}_4} \quad (\text{B7})$$

which is very important, and will be also used in second order renormalization. The first-order renormalization can be obtained by the mean field approximation:

$$\langle [\psi_{\mathbf{k}}, H']; \psi_{\mathbf{k}'}^\dagger \rangle_\omega \approx \sum_{\{\mathbf{k}_i\}} (V_{\mathbf{k}_2, \mathbf{k}}^{(k, k_2)} + V_{\mathbf{k}, \mathbf{k}_2}^{(k, k_2)}) \langle \psi_{\mathbf{k}_2}^\dagger \psi_{\mathbf{k}_2} \rangle \langle \psi_{\mathbf{k}}; \psi_{\mathbf{k}'}^\dagger \rangle_\omega$$

$$\approx \Sigma_{H'}^{(1)}(\mathbf{k}) \langle \psi_{\mathbf{k}}; \psi_{\mathbf{k}'}^\dagger \rangle_\omega \quad (\text{B8})$$

where $\Sigma_{H'}^{(1)}(\mathbf{k}) = \sum_{\mathbf{k}_2} V_{(\mathbf{k}_2, \mathbf{k})}^{(k, k_2)} \langle \psi_{\mathbf{k}_2}^\dagger \psi_{\mathbf{k}_2} \rangle^0$ is the first-order self-energy, $\langle \psi_{\mathbf{k}_2}^\dagger \psi_{\mathbf{k}_2} \rangle^0$ is the zeroth order population matrix.

$\Sigma_{H'}^{(1)}(\mathbf{k})$ is a 2×2 matrix can be written by: $\begin{pmatrix} \sigma_{11} & \sigma_{12} \\ \sigma_{21} & \sigma_{22} \end{pmatrix}$. Each element term has the explicit form:

$$\sigma_{11} = \frac{-J}{N_L} \sum_{\mathbf{k}_1} (\gamma_0 \langle b_{\mathbf{k}_1}^\dagger b_{\mathbf{k}_1} \rangle - \frac{1}{2} \gamma_{\mathbf{k}_1}^* \langle b_{\mathbf{k}_1}^\dagger a_{\mathbf{k}_1} \rangle - \frac{1}{2} \gamma_{\mathbf{k}_1} \langle a_{\mathbf{k}_1}^\dagger b_{\mathbf{k}_1} \rangle),$$

$$\sigma_{12} = \frac{-J}{N_L} \sum_{\mathbf{k}_1} (\gamma_{\mathbf{k}-\mathbf{k}_1} \langle b_{\mathbf{k}_1}^\dagger a_{\mathbf{k}_1} \rangle - \frac{1}{2} \gamma_{\mathbf{k}} \langle b_{\mathbf{k}_1}^\dagger b_{\mathbf{k}_1} \rangle - \frac{1}{2} \gamma_{\mathbf{k}} \langle a_{\mathbf{k}_1}^\dagger a_{\mathbf{k}_1} \rangle),$$

$$\sigma_{21} = \frac{-J}{N_L} \sum_{\mathbf{k}_1} (\gamma_{\mathbf{k}_1-\mathbf{k}} \langle a_{\mathbf{k}_1}^\dagger b_{\mathbf{k}_1} \rangle - \frac{1}{2} \gamma_{\mathbf{k}}^* \langle a_{\mathbf{k}_1}^\dagger a_{\mathbf{k}_1} \rangle - \frac{1}{2} \gamma_{\mathbf{k}}^* \langle b_{\mathbf{k}_1}^\dagger b_{\mathbf{k}_1} \rangle),$$

$$\sigma_{22} = \frac{-J}{N_L} \sum_{\mathbf{k}_1} (\gamma_0 \langle a_{\mathbf{k}_1}^\dagger a_{\mathbf{k}_1} \rangle - \frac{1}{2} \gamma_{\mathbf{k}_1} \langle a_{\mathbf{k}_1}^\dagger b_{\mathbf{k}_1} \rangle - \frac{1}{2} \gamma_{\mathbf{k}_1}^* \langle b_{\mathbf{k}_1}^\dagger a_{\mathbf{k}_1} \rangle). \quad (\text{B9})$$

The expectation value can be calculated by magnon statistics. The grand partition function has the form $Z = e^{-\beta E_G} \text{Tr}(e^{-\beta H_0})$, where $E_G = -3JS^2 N_L$ is the energy of ferromagnetic ground state, H_0 is the noninteracting magnon Hamiltonian. In eigenmode basis, $H_0 = \omega_{d_{\mathbf{k}}} d_{\mathbf{k}}^\dagger d_{\mathbf{k}} + \omega_{u_{\mathbf{k}}} u_{\mathbf{k}}^\dagger u_{\mathbf{k}}$, and $\psi_{\mathbf{k}} = U d_{\mathbf{k}}$, where U is the unitary matrix of basis transformation. We have:

$$\begin{pmatrix} a_{\mathbf{k}} \\ b_{\mathbf{k}} \end{pmatrix} = \frac{1}{\sqrt{2}} \begin{pmatrix} \sqrt{1 + \frac{B}{A}} e^{i\frac{\phi_{\mathbf{k}}}{2}} & \sqrt{1 - \frac{B}{A}} e^{i\frac{\phi_{\mathbf{k}}}{2}} \\ \sqrt{1 - \frac{B}{A}} e^{-i\frac{\phi_{\mathbf{k}}}{2}} & -\sqrt{1 + \frac{B}{A}} e^{-i\frac{\phi_{\mathbf{k}}}{2}} \end{pmatrix} \begin{pmatrix} d_{\mathbf{k}} \\ u_{\mathbf{k}} \end{pmatrix} \quad (\text{B10})$$

where $A = \sqrt{(\frac{2D\beta_{\mathbf{k}}}{J})^2 + |\gamma_{\mathbf{k}}|^2}$, and $B = \frac{2D\beta_{\mathbf{k}}}{J}$ are functions of wave vector \mathbf{k} . We obtain the averages of population operators from the grand canonical ensemble:

$$\langle a_{\mathbf{k}}^\dagger a_{\mathbf{k}} \rangle = \frac{1}{2} \left(1 + \frac{B}{A}\right) \langle d_{\mathbf{k}}^\dagger d_{\mathbf{k}} \rangle + \frac{1}{2} \left(1 - \frac{B}{A}\right) \langle u_{\mathbf{k}}^\dagger u_{\mathbf{k}} \rangle$$

$$= \frac{1}{2} \left(1 + \frac{B}{A}\right) f(\omega_{d_{\mathbf{k}}}) + \frac{1}{2} \left(1 - \frac{B}{A}\right) f(\omega_{u_{\mathbf{k}}}),$$

$$\langle b_{\mathbf{k}}^\dagger b_{\mathbf{k}} \rangle = \frac{1}{2} \left(1 - \frac{B}{A}\right) f(\omega_{d_{\mathbf{k}}}) + \frac{1}{2} \left(1 + \frac{B}{A}\right) f(\omega_{u_{\mathbf{k}}}),$$

$$\langle a_{\mathbf{k}}^\dagger b_{\mathbf{k}} \rangle = \langle b_{\mathbf{k}}^\dagger a_{\mathbf{k}} \rangle^* = \frac{1}{2} e^{-i\phi_{\mathbf{k}}} \sqrt{1 - \frac{B^2}{A^2}} \langle d_{\mathbf{k}}^\dagger d_{\mathbf{k}} - u_{\mathbf{k}}^\dagger u_{\mathbf{k}} \rangle$$

$$= \frac{1}{2} e^{-i\phi_{\mathbf{k}}} \sqrt{1 - \frac{B^2}{A^2}} (f(\omega_{d_{\mathbf{k}}}) - f(\omega_{u_{\mathbf{k}}})) \quad (\text{B11})$$

In first-order renormalization, we have to include the contributions from quartic DM interactions. We conclude a diagonal 2×2 self-energy matrix $\Sigma_{DM}^{(1)}(\mathbf{k}) = \begin{pmatrix} \sigma'_{11} & 0 \\ 0 & \sigma'_{22} \end{pmatrix}$. The diagonal matrix elements have the explicit forms $\sigma'_{11} = \sum_{\mathbf{k}_1} D_{(\mathbf{k}, \mathbf{k}_1)}^{(k_1, k)} \langle a_{\mathbf{k}_1}^\dagger a_{\mathbf{k}_1} \rangle$, and $\sigma'_{22} = -\sum_{\mathbf{k}_1} D_{(\mathbf{k}, \mathbf{k}_1)}^{(k_1, k)} \langle b_{\mathbf{k}_1}^\dagger b_{\mathbf{k}_1} \rangle$, where $D_{(\mathbf{k}, \mathbf{k}_1)}^{(k_1, k)} = D_{\mathbf{k}, \mathbf{k}_1}^{k_1, k} + D_{\mathbf{k}, \mathbf{k}_1}^{k, k_1} + D_{\mathbf{k}_1, \mathbf{k}}^{k_1, k} + D_{\mathbf{k}_1, \mathbf{k}}^{k, k_1}$ is symmetrized coefficient. We can have its explicit form $D_{(\mathbf{k}, \mathbf{k}_1)}^{(k_1, k)} = \frac{2D\beta_{\mathbf{k}}}{N_L} + \frac{2D\beta_{\mathbf{k}_1}}{N_L}$. Thus, we obtain:

$$\sigma'_{11} = \frac{D\beta_{\mathbf{k}}}{N_L} \sum_{\mathbf{k}_1} (f(\omega_{d_{\mathbf{k}_1}}) + f(\omega_{u_{\mathbf{k}_1}}))$$

$$+ \frac{D}{N_L} \sum_{\mathbf{k}_1} \frac{\beta_{\mathbf{k}_1} B}{A} (f(\omega_{d_{\mathbf{k}_1}}) - f(\omega_{u_{\mathbf{k}_1}}))$$

$$\sigma'_{22} = -\frac{D\beta_{\mathbf{k}}}{N_L} \sum_{\mathbf{k}_1} (f(\omega_{d_{\mathbf{k}_1}}) + f(\omega_{u_{\mathbf{k}_1}}))$$

$$+ \frac{D}{N_L} \sum_{\mathbf{k}_1} \frac{\beta_{\mathbf{k}_1} B}{A} (f(\omega_{d_{\mathbf{k}_1}}) - f(\omega_{u_{\mathbf{k}_1}})) \quad (\text{B12})$$

We can see that $\sigma'_{11} \neq \sigma'_{22}$, this term will contribute the effective Haldane mass. Finally, we obtain the total first-order self-energy, which is given by:

$$\Sigma_{H'}^{(1)}(\mathbf{k}) + \Sigma_{DM}^{(1)}(\mathbf{k}) = \frac{J}{2N_L} \sum_{\mathbf{k}_1} \begin{pmatrix} \Delta_1(\mathbf{k}_1) - \gamma_0 \Theta_b(\mathbf{k}_1) + \delta_m & \gamma_{\mathbf{k}} \Theta^+(\mathbf{k}_1) - \gamma_{\mathbf{k}-\mathbf{k}_1} e^{i\phi_{\mathbf{k}_1}} \Delta_2(\mathbf{k}_1) \\ \gamma_{\mathbf{k}}^* \Theta^+(\mathbf{k}_1) - \gamma_{\mathbf{k}_1-\mathbf{k}} e^{-i\phi_{\mathbf{k}_1}} \Delta_2(\mathbf{k}_1) & \Delta_1(\mathbf{k}_1) - \gamma_0 \Theta_a(\mathbf{k}_1) - \delta_m \end{pmatrix} \quad (\text{B13})$$

where we have the terms:

$$\begin{aligned} \Delta_1(\mathbf{k}_1) &= \left(|\gamma_{\mathbf{k}_1}| \sqrt{1 - \frac{B^2}{A^2}} + \frac{B^2}{A} \right) \Theta^-(\mathbf{k}_1), \\ \Delta_2(\mathbf{k}_1) &= \sqrt{1 - \frac{B^2}{A^2}} \Theta^-(\mathbf{k}_1), \\ \Theta_b(\mathbf{k}_1) &= \Theta^+(\mathbf{k}_1) - \frac{B}{A} \Theta^-(\mathbf{k}_1), \\ \Theta_a(\mathbf{k}_1) &= \Theta^+(\mathbf{k}_1) + \frac{B}{A} \Theta^-(\mathbf{k}_1), \end{aligned} \quad (\text{B14})$$

where $\Theta^+(\mathbf{k}) = f(\omega_{d_{\mathbf{k}}}) + f(\omega_{u_{\mathbf{k}}})$, $\Theta^-(\mathbf{k}) = f(\omega_{d_{\mathbf{k}}}) - f(\omega_{u_{\mathbf{k}}})$, and $\delta_m = \frac{2D\beta_{\mathbf{k}}}{J} \Theta^+(\mathbf{k}_1)$ is the interaction-induced

Haldane mass term. The DMI changes the population balances between $\langle a_{\mathbf{k}}^\dagger a_{\mathbf{k}} \rangle$ and $\langle b_{\mathbf{k}}^\dagger b_{\mathbf{k}} \rangle$, which can not be neglect around the Dirac point ($\frac{B}{A} = 1$). When DMI parameter D is zero or near the Γ point ($B \approx 0$), we have a simpler unitary transform matrix, which is given by:

$$\begin{pmatrix} a_{\mathbf{k}} \\ b_{\mathbf{k}} \end{pmatrix} \approx \frac{1}{\sqrt{2}} \begin{pmatrix} e^{i\frac{\phi_{\mathbf{k}}}{2}} & e^{i\frac{\phi_{\mathbf{k}}}{2}} \\ e^{-i\frac{\phi_{\mathbf{k}}}{2}} & -e^{-i\frac{\phi_{\mathbf{k}}}{2}} \end{pmatrix} \begin{pmatrix} d_{\mathbf{k}} \\ u_{\mathbf{k}} \end{pmatrix}. \quad (\text{B15})$$

In the low temperature approximation, all thermal excited magnons mainly populate around the Γ point of the lower band, where we have $B \approx 0$, $f(\omega_{u_{\mathbf{k}}}) = 0$, $\delta_m \approx 0$ and $\Theta^+(\mathbf{k}_1) = \Delta(\mathbf{k}_1) = f(\omega_{d_{\mathbf{k}_1}})$. The first-order self-energy at low temperature is thus given by:

$$\Sigma_{H'}^{(1)}(\mathbf{k}) = \frac{J}{2N_L} \sum_{\mathbf{k}_1} f(\omega_{\mathbf{k}_1}) \begin{pmatrix} \text{Re}(\gamma_{\mathbf{k}_1} e^{-i\phi_{\mathbf{k}_1}}) - \gamma_0 & \gamma_{\mathbf{k}} - \gamma_{\mathbf{k}-\mathbf{k}_1} e^{i\phi_{\mathbf{k}_1}} \\ \gamma_{\mathbf{k}}^* - \gamma_{\mathbf{k}_1-\mathbf{k}} e^{-i\phi_{\mathbf{k}_1}} & \text{Re}(\gamma_{\mathbf{k}_1} e^{-i\phi_{\mathbf{k}_1}}) - \gamma_0 \end{pmatrix} \approx -\frac{J}{2N_L} \sum_{\mathbf{k}_1} \frac{\omega_{\mathbf{k}_1}}{3JS} f(\omega_{\mathbf{k}_1}) \begin{pmatrix} 3 & -\gamma_{\mathbf{k}} \\ -\gamma_{\mathbf{k}}^* & 3 \end{pmatrix} \quad (\text{B16})$$

where $\text{Re}(\gamma_{\mathbf{k}_1} e^{-i\phi_{\mathbf{k}_1}}) = |\gamma_{\mathbf{k}_1}|$, and $1 - \gamma_{\mathbf{k}-\mathbf{k}_1} e^{i\phi_{\mathbf{k}_1}} / \gamma_{\mathbf{k}} \approx 1 - \gamma_{-\mathbf{k}_1} e^{i\phi_{\mathbf{k}_1}} / \gamma_0 = 1 - |\gamma_{\mathbf{k}_1}| / \gamma_0$ are employed. In the low temperature, the magnon excitations only exist around the zone center. We can use isotropic approximation and the magnon band has quadratic expression $\omega_{\mathbf{k}} = c_2 k^2$. The summation can

be written as:

$$\begin{aligned} \frac{1}{N_L} \sum_{\mathbf{k}_1} \omega_{\mathbf{k}_1} f(\omega_{\mathbf{k}_1}) &= \frac{1}{N_L} \sum_{\mathbf{k}_1} \frac{c_2 k_1^2}{e^{\omega_{\mathbf{k}_1} \beta} - 1} \\ &= \frac{A}{(2\pi)^2} \sum_{n=1}^{+\infty} \int d^2 \mathbf{k}_1 c_2 k_1^2 e^{-n\beta c_2 k_1^2} \\ &= \frac{A}{4\pi\beta^2 c_2} \sum_{n=1}^{+\infty} \frac{1}{n^2} = \frac{Ak_B^2}{4\pi c_2} \zeta(2) T^2, \end{aligned} \quad (\text{B17})$$

where $\frac{1}{N_L} \sum_{\mathbf{k}_1} = \frac{A}{(2\pi)^2} \int_{BZ} d^2 \mathbf{k}_1$ with A is the area of the primitive unitcell, $\zeta(p) = \sum_{n=1}^{+\infty} \frac{1}{n^p}$ is Riemann zeta function. When $p = 2$, $\zeta(2) = \frac{\pi^2}{6}$, and self-energy $\Sigma_{\mathbf{k}}^{(1)} = -\frac{A\pi k_B^2}{24J^2 S^3} T^2 H_0(\mathbf{k})$. One can see that the renormalization magnitude is proportional to T^2 at low temperature approximation.

Appendix C: Second-order renormalization of magnon band

We here to derive the second-order self-energy in weakly interacting magnon system. By the Eq. (B2), we have the Green's functions equation of motion:

$$\omega \langle [\psi_{\mathbf{k}}, H']; \psi_{\mathbf{k}'}^\dagger \rangle_\omega = \langle [[\psi_{\mathbf{k}}, H'], \psi_{\mathbf{k}'}^\dagger] \rangle + \langle [[\psi_{\mathbf{k}}, H'], H]; \psi_{\mathbf{k}'}^\dagger \rangle_\omega. \quad (\text{C1})$$

We have $[\psi_{\mathbf{k}}, H'] = \sum_{\{k_i\}} V_{k_3, k_4}^{k_1, k_2} [\psi_{\mathbf{k}}, \psi_{\mathbf{k}_1}^\dagger \psi_{\mathbf{k}_2}^\dagger \psi_{\mathbf{k}_3} \psi_{\mathbf{k}_4}] = \sum_{\{k_i\}} V_{k_3, k_4}^{(k, k_2)} \psi_{\mathbf{k}_2}^\dagger \psi_{\mathbf{k}_3} \psi_{\mathbf{k}_4} = \frac{1}{2} \sum_{\{k_i\}} V_{(k_3, k_4)}^{(k, k_2)} \psi_{\mathbf{k}_2}^\dagger \psi_{\mathbf{k}_3} \psi_{\mathbf{k}_4}$. For the last expression, we split the original form and relabel the indices for the symmetric interaction matrix $V_{(k_3, k_4)}^{(k, k_2)}$. We now transform above equation to

$$\frac{1}{2} \sum_{\{k_i\}} V_{(k_3, k_4)}^{(k, k_2)} \omega \langle \psi_{\mathbf{k}_2}^\dagger \psi_{\mathbf{k}_3} \psi_{\mathbf{k}_4}; \psi_{\mathbf{k}'}^\dagger \rangle_\omega = \frac{1}{2} \sum_{\{k_i\}} V_{(k_3, k_4)}^{(k, k_2)} \langle [\psi_{\mathbf{k}_2}^\dagger \psi_{\mathbf{k}_3} \psi_{\mathbf{k}_4}; \psi_{\mathbf{k}'}^\dagger] \rangle + \frac{1}{2} \sum_{\{k_i\}} V_{(k_3, k_4)}^{(k, k_2)} \langle [\psi_{\mathbf{k}_2}^\dagger \psi_{\mathbf{k}_3} \psi_{\mathbf{k}_4}, H]; \psi_{\mathbf{k}'}^\dagger \rangle_\omega. \quad (\text{C2})$$

We can neglect the summation first and focus on equation of motion of $\Psi_{\mathbf{k}_2}^\dagger \Psi_{\mathbf{k}_3} \Psi_{\mathbf{k}_4}$:

$$\omega \langle \Psi_{\mathbf{k}_2}^\dagger \Psi_{\mathbf{k}_3} \Psi_{\mathbf{k}_4}; \Psi_{\mathbf{k}'}^\dagger \rangle \omega = \langle [\Psi_{\mathbf{k}_2}^\dagger \Psi_{\mathbf{k}_3} \Psi_{\mathbf{k}_4}, \Psi_{\mathbf{k}'}^\dagger] \rangle + \langle [\Psi_{\mathbf{k}_2}^\dagger \Psi_{\mathbf{k}_3} \Psi_{\mathbf{k}_4}, H]; \Psi_{\mathbf{k}'}^\dagger \rangle \omega. \quad (\text{C3})$$

We expand the the first term in the RHS of above equation, which is the a commutator. From the Eq. (B7)

$$\langle [\Psi_{\mathbf{k}_2}^\dagger \Psi_{\mathbf{k}_3} \Psi_{\mathbf{k}_4}, \Psi_{\mathbf{k}'}^\dagger] \rangle \approx \langle \Psi_{\mathbf{k}_2}^\dagger \Psi_{\mathbf{k}_4} \rangle \delta_{\mathbf{k}_2, \mathbf{k}_4} \delta_{\mathbf{k}_3, \mathbf{k}'} + \langle \Psi_{\mathbf{k}_2}^\dagger \Psi_{\mathbf{k}_3} \rangle \delta_{\mathbf{k}_2, \mathbf{k}_3} \delta_{\mathbf{k}_4, \mathbf{k}'}, \quad (\text{C4})$$

The second term in Eq. (C3) is little bit complicated. We spilt the commutator $[\Psi_{\mathbf{k}_2}^\dagger \Psi_{\mathbf{k}_3} \Psi_{\mathbf{k}_4}, H]$ into two parts by separate the $H = H_0 + H'$, and obtain:

$$[\Psi_{\mathbf{k}_2}^\dagger \Psi_{\mathbf{k}_3} \Psi_{\mathbf{k}_4}, H_0] = \Psi_{\mathbf{k}_2}^\dagger \Psi_{\mathbf{k}_3} M_{\mathbf{k}_4} \Psi_{\mathbf{k}_4} + \Psi_{\mathbf{k}_2}^\dagger M_{\mathbf{k}_3} \Psi_{\mathbf{k}_3} \Psi_{\mathbf{k}_4} - \Psi_{\mathbf{k}_2}^\dagger M_{\mathbf{k}_2} \Psi_{\mathbf{k}_3} \Psi_{\mathbf{k}_4} \quad (\text{C5})$$

where the $M_{\mathbf{k}} \Psi_{\mathbf{k}}$ gives rise to the factors related to the magnon spectrum. We define a tensor with the symbol \mathcal{M} , which is the function $\mathcal{M} = \mathcal{M}(\mathbf{k}_2, \mathbf{k}_3, \mathbf{k}_4)$. We has the transformation $Q'_{a,bc} = \sum_{b,e,f} \mathcal{M}_{b,ef}^{a,bc} Q_{a,bc}$. Where $Q' = \Psi_{\mathbf{k}_2}^\dagger \Psi_{\mathbf{k}_3} M_{\mathbf{k}_4} \Psi_{\mathbf{k}_4} + \Psi_{\mathbf{k}_2}^\dagger M_{\mathbf{k}_3} \Psi_{\mathbf{k}_3} \Psi_{\mathbf{k}_4} - \Psi_{\mathbf{k}_2}^\dagger M_{\mathbf{k}_2} \Psi_{\mathbf{k}_3} \Psi_{\mathbf{k}_4}$, $Q_{a,bc} = \Psi_{\mathbf{k}_2}^\dagger \Psi_{\mathbf{k}_3} \Psi_{\mathbf{k}_4}$, and a, b and c are integers in $\{1, 2\}$ indexed the components of the quantity. For instance, $Q_{1,11} = a_{\mathbf{k}_2}^\dagger a_{\mathbf{k}_3} a_{\mathbf{k}_4}$, $Q_{1,21} = a_{\mathbf{k}_2}^\dagger b_{\mathbf{k}_3} a_{\mathbf{k}_4}$. Thus we can have a neat expression which is:

$$[[\Psi_{\mathbf{k}}, H'], H_0] = \frac{1}{2} \sum_{\{\mathbf{k}_i\}} V_{(\mathbf{k}_3, \mathbf{k}_4)}^{(\mathbf{k}, \mathbf{k}_2)} \sum_{b,e,f} \mathcal{M}_{b,ef}^{a,bc} Q_{a,bc} = \frac{1}{2} \sum_{\{\mathbf{k}_i\}} V_{(\mathbf{k}_3, \mathbf{k}_4)}^{(\mathbf{k}, \mathbf{k}_2)} \mathcal{M} \Psi_{\mathbf{k}_2}^\dagger \Psi_{\mathbf{k}_3} \Psi_{\mathbf{k}_4} \quad (\text{C6})$$

Thus we have $\langle [\Psi_{\mathbf{k}_2}^\dagger \Psi_{\mathbf{k}_3} \Psi_{\mathbf{k}_4}, H_0]; \Psi_{\mathbf{k}'}^\dagger \rangle \omega = \mathcal{M} \langle \Psi_{\mathbf{k}_2}^\dagger \Psi_{\mathbf{k}_3} \Psi_{\mathbf{k}_4}; \Psi_{\mathbf{k}'}^\dagger \rangle \omega$. Now we focus on the term $[\Psi_{\mathbf{k}_2}^\dagger \Psi_{\mathbf{k}_3} \Psi_{\mathbf{k}_4}, H']$, It gives rise more complicate terms written as:

$$\begin{aligned} [\Psi_{\mathbf{k}_2}^\dagger \Psi_{\mathbf{k}_3} \Psi_{\mathbf{k}_4}, H'] &= - \sum_{\mathbf{k}'_i} V_{(\mathbf{k}'_3, \mathbf{k}_2)}^{(\mathbf{k}_1, \mathbf{k}'_2)} \Psi_{\mathbf{k}'_1}^\dagger \Psi_{\mathbf{k}'_2}^\dagger \Psi_{\mathbf{k}'_3} \Psi_{\mathbf{k}_3} \Psi_{\mathbf{k}_4} + \sum_{\mathbf{k}'_i} V_{(\mathbf{k}_3, \mathbf{k}'_4)}^{(\mathbf{k}_3, \mathbf{k}'_2)} \Psi_{\mathbf{k}_2}^\dagger \Psi_{\mathbf{k}'_2}^\dagger \Psi_{\mathbf{k}'_3} \Psi_{\mathbf{k}_3} \Psi_{\mathbf{k}_4} \\ &+ \sum_{\mathbf{k}'_i} V_{(\mathbf{k}'_3, \mathbf{k}'_4)}^{(\mathbf{k}_4, \mathbf{k}'_2)} \Psi_{\mathbf{k}_2}^\dagger \Psi_{\mathbf{k}'_2}^\dagger \Psi_{\mathbf{k}_3} \Psi_{\mathbf{k}'_3} \Psi_{\mathbf{k}'_4} + \sum_{\mathbf{k}'_i} V_{(\mathbf{k}'_3, \mathbf{k}'_4)}^{(\mathbf{k}_4, \mathbf{k}_3)} \Psi_{\mathbf{k}_2}^\dagger \Psi_{\mathbf{k}'_3} \Psi_{\mathbf{k}'_4}. \end{aligned} \quad (\text{C7})$$

We still employ the RPA, and consider about the all possible contractions. We have

$$\begin{aligned} \sum_{\mathbf{k}'_i} V_{(\mathbf{k}'_3, \mathbf{k}_2)}^{(\mathbf{k}_1, \mathbf{k}'_2)} \langle \Psi_{\mathbf{k}'_1}^\dagger \Psi_{\mathbf{k}'_2}^\dagger \Psi_{\mathbf{k}'_3} \Psi_{\mathbf{k}_3} \Psi_{\mathbf{k}_4}; \Psi_{\mathbf{k}'}^\dagger \rangle &\approx V_{(\mathbf{k}, \mathbf{k}_2)}^{(\mathbf{k}_4, \mathbf{k}_3)} \langle \Psi_{\mathbf{k}_3}^\dagger \Psi_{\mathbf{k}_3} \rangle \langle \Psi_{\mathbf{k}_4}^\dagger \Psi_{\mathbf{k}_4} \rangle \langle \Psi_{\mathbf{k}}; \Psi_{\mathbf{k}'}^\dagger \rangle + \sum_{\mathbf{k}'_3} V_{(\mathbf{k}'_3, \mathbf{k}_2)}^{(\mathbf{k}_4, \mathbf{k}'_3)} \delta_{\mathbf{k}_3, \mathbf{k}} \langle \Psi_{\mathbf{k}_4}^\dagger \Psi_{\mathbf{k}_4} \rangle \langle \Psi_{\mathbf{k}'_3}^\dagger \Psi_{\mathbf{k}'_3} \rangle \langle \Psi_{\mathbf{k}}; \Psi_{\mathbf{k}'}^\dagger \rangle \\ &+ \sum_{\mathbf{k}'_3} V_{(\mathbf{k}'_3, \mathbf{k}_2)}^{(\mathbf{k}_3, \mathbf{k}'_3)} \delta_{\mathbf{k}_4, \mathbf{k}} \langle \Psi_{\mathbf{k}_3}^\dagger \Psi_{\mathbf{k}_3} \rangle \langle \Psi_{\mathbf{k}'_3}^\dagger \Psi_{\mathbf{k}'_3} \rangle \langle \Psi_{\mathbf{k}}; \Psi_{\mathbf{k}'}^\dagger \rangle \end{aligned} \quad (\text{C8})$$

For the second and third terms in Eq (C4), we apply the same procedure:

$$\begin{aligned} &\sum_{\mathbf{k}'_i} V_{(\mathbf{k}'_3, \mathbf{k}'_4)}^{(\mathbf{k}_3, \mathbf{k}'_2)} \langle \Psi_{\mathbf{k}_2}^\dagger \Psi_{\mathbf{k}'_2}^\dagger \Psi_{\mathbf{k}'_3} \Psi_{\mathbf{k}'_4} \Psi_{\mathbf{k}_4}; \Psi_{\mathbf{k}'}^\dagger \rangle + \sum_{\mathbf{k}'_i} V_{(\mathbf{k}'_3, \mathbf{k}'_4)}^{(\mathbf{k}_4, \mathbf{k}'_2)} \langle \Psi_{\mathbf{k}_2}^\dagger \Psi_{\mathbf{k}'_2}^\dagger \Psi_{\mathbf{k}_3} \Psi_{\mathbf{k}'_3} \Psi_{\mathbf{k}'_4}; \Psi_{\mathbf{k}'}^\dagger \rangle \\ &= \sum_{\mathbf{k}'_2} V_{(\mathbf{k}'_2, \mathbf{k}_2)}^{(\mathbf{k}_3, \mathbf{k}'_2)} \delta_{\mathbf{k}_4, \mathbf{k}} \langle \Psi_{\mathbf{k}_2}^\dagger \Psi_{\mathbf{k}_2} \rangle \langle \Psi_{\mathbf{k}'_2}^\dagger \Psi_{\mathbf{k}'_2} \rangle \langle \Psi_{\mathbf{k}}; \Psi_{\mathbf{k}'}^\dagger \rangle + \sum_{\mathbf{k}'_2} V_{(\mathbf{k}'_2, \mathbf{k})}^{(\mathbf{k}_3, \mathbf{k}'_2)} \delta_{\mathbf{k}_4, \mathbf{k}_2} \langle \Psi_{\mathbf{k}_2}^\dagger \Psi_{\mathbf{k}_2} \rangle \langle \Psi_{\mathbf{k}'_2}^\dagger \Psi_{\mathbf{k}'_2} \rangle \langle \Psi_{\mathbf{k}}; \Psi_{\mathbf{k}'}^\dagger \rangle \\ &= V_{(\mathbf{k}_2, \mathbf{k})}^{(\mathbf{k}_3, \mathbf{k}_4)} \langle \Psi_{\mathbf{k}_2}^\dagger \Psi_{\mathbf{k}_2} \rangle \langle \Psi_{\mathbf{k}_4}^\dagger \Psi_{\mathbf{k}_4} \rangle \langle \Psi_{\mathbf{k}}; \Psi_{\mathbf{k}'}^\dagger \rangle + \sum_{\mathbf{k}'_2} V_{(\mathbf{k}'_2, \mathbf{k}_2)}^{(\mathbf{k}_4, \mathbf{k}'_2)} \delta_{\mathbf{k}_3, \mathbf{k}} \langle \Psi_{\mathbf{k}_2}^\dagger \Psi_{\mathbf{k}_2} \rangle \langle \Psi_{\mathbf{k}'_2}^\dagger \Psi_{\mathbf{k}'_2} \rangle \langle \Psi_{\mathbf{k}}; \Psi_{\mathbf{k}'}^\dagger \rangle \\ &= V_{(\mathbf{k}_2, \mathbf{k})}^{(\mathbf{k}_3, \mathbf{k}_4)} \langle \Psi_{\mathbf{k}_2}^\dagger \Psi_{\mathbf{k}_2} \rangle \langle \Psi_{\mathbf{k}_3}^\dagger \Psi_{\mathbf{k}_3} \rangle \langle \Psi_{\mathbf{k}}; \Psi_{\mathbf{k}'}^\dagger \rangle + \sum_{\mathbf{k}'_2} V_{(\mathbf{k}'_2, \mathbf{k})}^{(\mathbf{k}_4, \mathbf{k}'_2)} \delta_{\mathbf{k}_3, \mathbf{k}_2} \langle \Psi_{\mathbf{k}_2}^\dagger \Psi_{\mathbf{k}_2} \rangle \langle \Psi_{\mathbf{k}'_2}^\dagger \Psi_{\mathbf{k}'_2} \rangle \langle \Psi_{\mathbf{k}}; \Psi_{\mathbf{k}'}^\dagger \rangle \end{aligned} \quad (\text{C9})$$

The first and fourth terms in the bracket cancel the last two terms in Eq. (C8), the second term:

$$\sum_{\mathbf{k}'_2} V_{(\mathbf{k}'_2, \mathbf{k})}^{(\mathbf{k}_3, \mathbf{k}'_2)} \delta_{\mathbf{k}_4, \mathbf{k}_2} \langle \Psi_{\mathbf{k}_2}^\dagger \Psi_{\mathbf{k}_2} \rangle \langle \Psi_{\mathbf{k}'_2}^\dagger \Psi_{\mathbf{k}'_2} \rangle \langle \Psi_{\mathbf{k}}; \Psi_{\mathbf{k}'}^\dagger \rangle = \delta_{\mathbf{k}_4, \mathbf{k}_2} \langle \Psi_{\mathbf{k}_2}^\dagger \Psi_{\mathbf{k}_2} \rangle \Sigma_{\mathbf{k}}^{(1)} \langle \Psi_{\mathbf{k}}; \Psi_{\mathbf{k}'}^\dagger \rangle \quad (\text{C10})$$

and we obtain the similar result for the last term $\delta_{\mathbf{k}_3, \mathbf{k}_2} \langle \Psi_{\mathbf{k}_2}^\dagger \Psi_{\mathbf{k}_2} \rangle \Sigma_{\mathbf{k}}^{(1)} \langle \Psi_{\mathbf{k}}; \Psi_{\mathbf{k}'}^\dagger \rangle$. Finally, we calculate the last term in Eq. (C4), which can be written as:

$$\sum_{\mathbf{k}'_i} V_{(\mathbf{k}'_3, \mathbf{k}'_4)}^{(\mathbf{k}_4, \mathbf{k}_3)} \langle \Psi_{\mathbf{k}_2}^\dagger \Psi_{\mathbf{k}'_3} \Psi_{\mathbf{k}'_4}; \Psi_{\mathbf{k}'}^\dagger \rangle = V_{(\mathbf{k}_2, \mathbf{k})}^{(\mathbf{k}_4, \mathbf{k}_3)} \langle \Psi_{\mathbf{k}_2}^\dagger \Psi_{\mathbf{k}_2} \rangle \langle \Psi_{\mathbf{k}}; \Psi_{\mathbf{k}'}^\dagger \rangle \omega \quad (\text{C11})$$

Combining the Eqs (C8–C11), we obtain

$$\langle [\Psi_{k_2}^\dagger \Psi_{k_3} \Psi_{k_4}, H']; \Psi_{k'}^\dagger \rangle_\omega = \left(V_{(k_2, k)}^{(k_4, k_3)} (n_{k_2} (1 + n_{k_3} + n_{k_4}) - n_{k_3} n_{k_4}) + (\delta_{k_4, k_2} + \delta_{k_3, k_2}) n_{k_2} \Sigma_k^{(1)} \right) \langle \Psi_k; \Psi_{k'}^\dagger \rangle_\omega \quad (C12)$$

where n_{k_i} is short for $\langle \Psi_{k_i}^\dagger \Psi_{k_i} \rangle$. We can replace the Green's function $\langle \Psi_k; \Psi_{k'}^\dagger \rangle_\omega$ with free particle one $\langle \Psi_k; \Psi_{k'}^\dagger \rangle_\omega^0$ in this order. We note it that for the second-order renormalization, it is very convenient to write down the full expression in eigen-mode space. We will do it later using a unitary transformation. We have the expression:

$$\begin{aligned} (\omega - \mathcal{M}) \langle \Psi_{k_2}^\dagger \Psi_{k_3} \Psi_{k_4}; \Psi_{k'}^\dagger \rangle_\omega &= n_{k_4} \delta_{k_2, k_4} \delta_{k_3, k'} + n_{k_3} \delta_{k_2, k_3} \delta_{k_4, k'} + \langle [\Psi_{k_2}^\dagger \Psi_{k_3} \Psi_{k_4}, H']; \Psi_{k'}^\dagger \rangle_\omega \\ &= n_{k_2} (\delta_{k_2, k_4} \delta_{k_3, k'} + \delta_{k_2, k_3} \delta_{k_4, k'}) + \left(V_{(k_2, k)}^{(k_4, k_3)} (n_{k_2} (1 + n_{k_3} + n_{k_4}) - n_{k_3} n_{k_4}) + (\delta_{k_4, k_2} + \delta_{k_3, k_2}) n_{k_2} \Sigma_k^{(1)} \right) \langle \Psi_k; \Psi_{k'}^\dagger \rangle_\omega^0 \end{aligned} \quad (C13)$$

Thus the high-order renormalization effect can be summarized as:

$$\begin{aligned} \frac{1}{2} \sum_{k_i} V_{(k_3, k_4)}^{(k, k_2)} \langle \Psi_{k_2}^\dagger \Psi_{k_3} \Psi_{k_4}; \Psi_{k'}^\dagger \rangle_\omega &= \frac{1}{2} \sum_{k_i} V_{(k_3, k_4)}^{(k, k_2)} (\omega - \mathcal{M})^{-1} n_{k_2} (\delta_{k_2, k_4} \delta_{k_3, k'} + \delta_{k_2, k_3} \delta_{k_4, k'}) \\ &+ \frac{1}{2} \sum_{k_i} V_{(k_3, k_4)}^{(k, k_2)} (\omega - \mathcal{M})^{-1} \left(V_{(k_2, k)}^{(k_4, k_3)} (n_{k_2} (1 + n_{k_3} + n_{k_4}) - n_{k_3} n_{k_4}) + (\delta_{k_4, k_2} + \delta_{k_3, k_2}) n_{k_2} \Sigma_k^{(1)} \right) \langle \Psi_k; \Psi_{k'}^\dagger \rangle_\omega^0 \end{aligned} \quad (C14)$$

Where the first term in RHS can be simplified

$$\frac{1}{2} \sum_{k_i} V_{(k_3, k_4)}^{(k, k_2)} (\omega - \mathcal{M})^{-1} n_{k_2} (\delta_{k_2, k_4} \delta_{k_3, k'} + \delta_{k_2, k_3} \delta_{k_4, k'}) \approx \Sigma_k^{(1)} \langle \Psi_k; \Psi_{k'}^\dagger \rangle_\omega^0 \quad (C15)$$

using $(\omega - \mathcal{M})^{-1} n_{k_2} (\delta_{k_2, k_4} \delta_{k_3, k'} + \delta_{k_2, k_3} \delta_{k_4, k'}) = \frac{2n_{k_2}}{\omega - M(k')}$ and $\sum_{k_2} V_{(k_2, k)}^{(k, k_2)} n_{k_2} = \Sigma_k^{(1)}$. The second term in RHS:

$$\begin{aligned} \frac{1}{2} \sum_{k_i} V_{(k_3, k_4)}^{(k, k_2)} (\omega - \mathcal{M})^{-1} \left(V_{(k_2, k)}^{(k_4, k_3)} (n_{k_2} (1 + n_{k_3} + n_{k_4}) - n_{k_3} n_{k_4}) + (\delta_{k_4, k_2} + \delta_{k_3, k_2}) n_{k_2} \Sigma_k^{(1)} \right) \langle \Psi_k; \Psi_{k'}^\dagger \rangle_\omega^0 \\ = \frac{1}{2} \sum_{k_i} \frac{V_{(k_3, k_4)}^{(k, k_2)} V_{(k_2, k)}^{(k_4, k_3)} (n_{k_2} (1 + n_{k_3} + n_{k_4}) - n_{k_3} n_{k_4})}{\omega - \mathcal{M}} \langle \Psi_k; \Psi_{k'}^\dagger \rangle_\omega^0 + \langle \Psi_k; \Psi_{k'}^\dagger \rangle_\omega^0 (\Sigma_k^{(1)})^2 \langle \Psi_k; \Psi_{k'}^\dagger \rangle_\omega^0. \end{aligned} \quad (C16)$$

We drop $(\Sigma_k^{(1)})^2$ term, since it is just 2 loops of first-order renormalization and can be reducible. The second-order self-energy now have the expression:

$$\Sigma_k^{(2)} = \frac{1}{2} \sum_{\{k_i\}} \frac{V_{(k_3, k_4)}^{(k, k_2)} V_{(k_2, k)}^{(k_4, k_3)} (n_{k_2} (1 + n_{k_3} + n_{k_4}) - n_{k_3} n_{k_4})}{\omega_k + i\varepsilon - \mathcal{M}(k_2, k_3, k_4)} \quad (C17)$$

with replacing the ω by $\omega_k + i\varepsilon$ where the infinitesimal imaginary part is the argument of the retarded Green's function. we can separate $\Sigma_k^{(2)} = \Sigma_k^{(2)'} - i\Sigma_k^{(2)''}$, where the real part is the renormalization term and the imaginary part is the damping term.

Thus, we have the final Green's functions with second order renormalizations:

$$\begin{aligned} \langle \Psi_k; \Psi_{k'}^\dagger \rangle_{\omega + i\varepsilon} &= \frac{\langle [\Psi_k, \Psi_{k'}^\dagger] \rangle}{\omega + i\varepsilon - M_k} + \frac{1}{\omega + i\varepsilon - M_k} \Sigma_k^{(1)} \langle \Psi_k; \Psi_{k'}^\dagger \rangle^{(0)} + \frac{1}{\omega + i\varepsilon - M_k} \Sigma_k^{(2)} \langle \Psi_k; \Psi_{k'}^\dagger \rangle^{(0)} \\ &= \langle \Psi_k; \Psi_{k'}^\dagger \rangle_{\omega + i\varepsilon}^{(0)} + \langle \Psi_k; \Psi_{k'}^\dagger \rangle_{\omega + i\varepsilon}^{(0)} \Sigma_k^{(1)} \langle \Psi_k; \Psi_{k'}^\dagger \rangle_{\omega + i\varepsilon}^{(0)} + \langle \Psi_k; \Psi_{k'}^\dagger \rangle_{\omega + i\varepsilon}^{(0)} \Sigma_k^{(2)} (\omega_k + i\varepsilon) \langle \Psi_k; \Psi_{k'}^\dagger \rangle_{\omega + i\varepsilon}^{(0)}, \end{aligned} \quad (C18)$$

which follows the Dyson equation in spinor form. We have built the formalism for the many-body renormalization of a spinor. In order to calculate the spectrum structure, it is convenient to transform the sublattice basis to the eigen-mode basis by the unitary in Eq. (B15):

$$\begin{aligned} \langle d_k; d_{k'}^\dagger \rangle &= U^\dagger \langle \Psi_k; \Psi_{k'}^\dagger \rangle U \\ &= U^\dagger \langle \Psi_k; \Psi_{k'}^\dagger \rangle^{(0)} U + U^\dagger \langle \Psi_k; \Psi_{k'}^\dagger \rangle^{(0)} U U^\dagger \Sigma_k^{(1)} U U^\dagger \langle \Psi_k; \Psi_{k'}^\dagger \rangle^{(0)} U + U^\dagger \langle \Psi_k; \Psi_{k'}^\dagger \rangle^{(0)} U U^\dagger \Sigma_k^{(2)} U U^\dagger \langle \Psi_k; \Psi_{k'}^\dagger \rangle^{(0)} U \\ &= \langle d_k; d_{k'}^\dagger \rangle^0 + \langle d_k; d_{k'}^\dagger \rangle^0 U^\dagger \Sigma_k^{(1)} U \langle d_k; d_{k'}^\dagger \rangle^0 + \langle d_k; d_{k'}^\dagger \rangle^0 U^\dagger \Sigma_k^{(2)} U \langle d_k; d_{k'}^\dagger \rangle^0. \end{aligned} \quad (C19)$$

Calculation rules and interaction matrix—We notify the calculation rules, since there are plenty of matrices and scalars in the formulae. First, we define the commutator $[\psi_{\mathbf{k}}, \psi_{\mathbf{k}'}^\dagger]$ of spinors:

$$\begin{aligned} [\psi_{\mathbf{k}}, \psi_{\mathbf{k}'}^\dagger] &= \left[\begin{pmatrix} a_{\mathbf{k}} \\ b_{\mathbf{k}} \end{pmatrix}, \begin{pmatrix} a_{\mathbf{k}'}^\dagger & b_{\mathbf{k}'}^\dagger \end{pmatrix} \right] = \begin{pmatrix} [a_{\mathbf{k}}, a_{\mathbf{k}'}^\dagger] & [a_{\mathbf{k}}, b_{\mathbf{k}'}^\dagger] \\ [b_{\mathbf{k}}, a_{\mathbf{k}'}^\dagger] & [b_{\mathbf{k}}, b_{\mathbf{k}'}^\dagger] \end{pmatrix} = \delta_{\mathbf{k}, \mathbf{k}'} \mathbf{I} \\ \sum_{\mathbf{k}} \langle \psi_{\mathbf{k}}^\dagger \psi_{\mathbf{k}} \rangle &= \sum_{\mathbf{k}} \left(\langle a_{\mathbf{k}}^\dagger a_{\mathbf{k}} \rangle + \langle a_{\mathbf{k}}^\dagger b_{\mathbf{k}} \rangle + \langle b_{\mathbf{k}}^\dagger a_{\mathbf{k}} \rangle + \langle b_{\mathbf{k}}^\dagger b_{\mathbf{k}} \rangle \right) \\ \sum_{\mathbf{k}} \psi_{\mathbf{k}}^\dagger M_{\mathbf{k}} \psi_{\mathbf{k}} &= \sum_{\mathbf{k}} \left(M_{\mathbf{k}}^{11} a_{\mathbf{k}}^\dagger a_{\mathbf{k}} + M_{\mathbf{k}}^{12} a_{\mathbf{k}}^\dagger b_{\mathbf{k}} + M_{\mathbf{k}}^{21} b_{\mathbf{k}}^\dagger a_{\mathbf{k}} + M_{\mathbf{k}}^{22} b_{\mathbf{k}}^\dagger b_{\mathbf{k}} \right) \end{aligned} \quad (\text{C20})$$

We can see that in $\sum_{\mathbf{k}} \psi_{\mathbf{k}}^\dagger M_{\mathbf{k}} \psi_{\mathbf{k}}$, $M_{\mathbf{k}}^{ab}$ is always following the $\psi_{a,\mathbf{k}}^\dagger \psi_{b,\mathbf{k}}$, which is nothing but matrix multiplication. Thus, if we keep in mind that we always have this expansion rule in expressions which have the form $\psi_{\mathbf{k}}^\dagger A_{\mathbf{k}} \psi_{\mathbf{k}}$, then we can change the order to the form $A_{\mathbf{k}} \psi_{\mathbf{k}}^\dagger \psi_{\mathbf{k}}$. This is why the interaction Hamiltonian can be written in the form: $\sum_{\{k_i\}} V_{k_3, k_4}^{k_1, k_2} \psi_{k_1}^\dagger \psi_{k_2}^\dagger \psi_{k_3} \psi_{k_4}$. The reordering can bring a lot of conveniences in the formalism.

The interacting matrix $V_{k_3, k_4}^{k_1, k_2}$ is 4-dimensional matrix. The nonzero matrix elements from the interacting Hamiltonian are $V_{1,2}^{1,2} = -\frac{J}{N_L} \gamma_{k_4 - k_2}$, $V_{2,2}^{1,2} = \frac{J}{4N_L} \gamma_{k_4}$, $V_{1,1}^{2,1} = \frac{J}{4N_L} \gamma_{k_1}^*$, $V_{2,1}^{2,2} = \frac{J}{4N_L} \gamma_{k_4}^*$ and $V_{1,2}^{1,1} = \frac{J}{4N_L} \gamma_{k_4}$. We use a $V_{c,d}^{a,b}$ short for $V_{ck_3, dk_4}^{ak_1, bk_2}$, and $a, b, c, d \in \{1, 2\}$ are the labels for the two components of spinor $\psi_{\mathbf{k}} (\psi_{\mathbf{k}}^\dagger)$. One can check the first-order renormalization $\Sigma_{\mathbf{k}}^{(1)} = \sum_{k_2} V_{(k_2, k)}^{(k, k_2)} \langle \psi_{k_2}^\dagger \psi_{k_2} \rangle^0$. Since k_2 is a dummy index, and the summation (contraction) of k_2 leaves a 2x2 matrix. Inserting the each nonzero interacting element gives rise to the explicit form in Eq. (B9).

Appendix D: Interaction matrix element in eigen-mode basis

In order to calculate the second-order self-energy, we need to calculate the each matrix element. We have the retarded Green's function:

$$G_R(\mathbf{k}, \mathbf{k}'; \omega) = \langle \psi_{\mathbf{k}}; \psi_{\mathbf{k}'}^\dagger \rangle_\omega = \begin{pmatrix} \langle a_{\mathbf{k}}; a_{\mathbf{k}'}^\dagger \rangle_\omega & \langle a_{\mathbf{k}}; b_{\mathbf{k}'}^\dagger \rangle_\omega \\ \langle b_{\mathbf{k}}; a_{\mathbf{k}'}^\dagger \rangle_\omega & \langle b_{\mathbf{k}}; b_{\mathbf{k}'}^\dagger \rangle_\omega \end{pmatrix} \quad (\text{D1})$$

The equation of motion of Green's function can be written as

$$\begin{aligned} \omega \langle \psi_{\mathbf{k}}; \psi_{\mathbf{k}'}^\dagger \rangle_\omega &= \langle [\psi_{\mathbf{k}}, \psi_{\mathbf{k}'}^\dagger] \rangle + \langle [\psi_{\mathbf{k}}, H]; \psi_{\mathbf{k}'}^\dagger \rangle_\omega \\ &= \langle [\psi_{\mathbf{k}}, \psi_{\mathbf{k}'}^\dagger] \rangle + \langle [\psi_{\mathbf{k}}, H_0]; \psi_{\mathbf{k}'}^\dagger \rangle_\omega + \langle [\psi_{\mathbf{k}}, H']; \psi_{\mathbf{k}'}^\dagger \rangle_\omega. \end{aligned} \quad (\text{D2})$$

We have the $[\psi_{\mathbf{k}}, H']$, which can be written as:

$$\Phi_{\mathbf{k}} = [\psi_{\mathbf{k}}, H'] = -\frac{J}{4N_L} \sum_{k_2, k_3, k_4} \begin{pmatrix} 4\gamma_{k_4 - k_2} b_{k_2}^\dagger a_{k_3} b_{k_4} - \gamma_{k_2} b_{k_2}^\dagger b_{k_3} b_{k_4} - \gamma_{k_2}^* b_{k_2}^\dagger a_{k_3} a_{k_4} - 2\gamma_{k_4} a_{k_2}^\dagger a_{k_3} b_{k_4} \\ 4\gamma_{k_4 - k} a_{k_2}^\dagger a_{k_3} b_{k_4} - \gamma_{k_2} a_{k_2}^\dagger b_{k_3} b_{k_4} - \gamma_{k_2}^* a_{k_2}^\dagger a_{k_3} a_{k_4} - 2\gamma_{k_4}^* b_{k_2}^\dagger b_{k_3} a_{k_4} \end{pmatrix}. \quad (\text{D3})$$

We have the equation motion of $\Phi_{\mathbf{k}}$:

$$\omega \langle \Phi_{\mathbf{k}}; \psi_{\mathbf{k}'}^\dagger \rangle_\omega = \langle [\Phi_{\mathbf{k}}, \psi_{\mathbf{k}'}^\dagger] \rangle + \langle [\Phi_{\mathbf{k}}, H]; \psi_{\mathbf{k}'}^\dagger \rangle_\omega = \omega \begin{pmatrix} \langle \Phi_{\mathbf{k}}^1; a_{\mathbf{k}'}^\dagger \rangle_\omega & \langle \Phi_{\mathbf{k}}^1; b_{\mathbf{k}'}^\dagger \rangle_\omega \\ \langle \Phi_{\mathbf{k}}^2; a_{\mathbf{k}'}^\dagger \rangle_\omega & \langle \Phi_{\mathbf{k}}^2; b_{\mathbf{k}'}^\dagger \rangle_\omega \end{pmatrix} \quad (\text{D4})$$

Where $\langle [\Phi_{\mathbf{k}}, \psi_{\mathbf{k}'}^\dagger] \rangle$ has:

$$\begin{aligned} \langle \cdots \rangle_{11} &= -\frac{J}{4N_L} \sum_{k_2, k_3, k_4} 4\gamma_{k_4 - k_2} \langle b_{k_2}^\dagger b_{k_4} \rangle \delta_{k_3, k'} - \gamma_{k_2}^* \langle b_{k_2}^\dagger a_{k_3} \rangle \delta_{k_4, k'} + \langle b_{k_2}^\dagger a_{k_4} \rangle \delta_{k_3, k'} - 2\gamma_{k_4} \langle a_{k_2}^\dagger b_{k_4} \rangle \delta_{k_3, k'} \\ \langle \cdots \rangle_{12} &= -\frac{J}{4N_L} \sum_{k_2, k_3, k_4} 4\gamma_{k_4 - k_2} \langle b_{k_2}^\dagger a_{k_3} \rangle \delta_{k_4, k'} - \gamma_{k_2} \langle b_{k_2}^\dagger b_{k_3} \rangle \delta_{k_4, k'} + \langle b_{k_2}^\dagger b_{k_4} \rangle \delta_{k_3, k'} - 2\gamma_{k_4} \langle a_{k_2}^\dagger a_{k_3} \rangle \delta_{k_4, k'} \\ \langle \cdots \rangle_{21} &= -\frac{J}{4N_L} \sum_{k_2, k_3, k_4} 4\gamma_{k_4 - k} \langle a_{k_2}^\dagger b_{k_4} \rangle \delta_{k_3, k'} - \gamma_{k_2}^* \langle a_{k_2}^\dagger a_{k_3} \rangle \delta_{k_4, k'} + \langle a_{k_2}^\dagger a_{k_4} \rangle \delta_{k_3, k'} - 2\gamma_{k_4}^* \langle b_{k_2}^\dagger b_{k_3} \rangle \delta_{k_4, k'} \\ \langle \cdots \rangle_{22} &= -\frac{J}{4N_L} \sum_{k_2, k_3, k_4} 4\gamma_{k_4 - k} \langle a_{k_2}^\dagger a_{k_3} \rangle \delta_{k_4, k'} - \gamma_{k_2} \langle a_{k_2}^\dagger b_{k_3} \rangle \delta_{k_4, k'} + \langle a_{k_2}^\dagger b_{k_4} \rangle \delta_{k_3, k'} - 2\gamma_{k_4}^* \langle b_{k_2}^\dagger a_{k_4} \rangle \delta_{k_3, k'} \end{aligned} \quad (\text{D5})$$

One can see that each band has 8 scattering channels. We list the interaction matrix elements of each channel:

$$\begin{aligned}
V^{(1)} &= \frac{-J}{4N_L} (4\gamma_{k_4-k_2} U_{k_1}^{11*} U_{k_2}^{21*} U_{k_3}^{11} U_{k_4}^{21} - \gamma_{k_1} U_{k_1}^{11*} U_{k_2}^{21*} U_{k_3}^{21} U_{k_4}^{21} - \gamma_{k_1}^* U_{k_1}^{21*} U_{k_2}^{11*} U_{k_3}^{11} U_{k_4}^{11} - \gamma_{k_4}^* U_{k_1}^{21*} U_{k_2}^{21*} U_{k_3}^{21} U_{k_4}^{11} - \gamma_{k_4} U_{k_1}^{11*} U_{k_2}^{11*} U_{k_3}^{11} U_{k_4}^{21}) \\
V^{(2)} &= \frac{-J}{4N_L} (4\gamma_{k_4-k_2} U_{k_1}^{12*} U_{k_2}^{22*} U_{k_3}^{12} U_{k_4}^{22} - \gamma_{k_1} U_{k_1}^{12*} U_{k_2}^{22*} U_{k_3}^{22} U_{k_4}^{22} - \gamma_{k_1}^* U_{k_1}^{22*} U_{k_2}^{12*} U_{k_3}^{12} U_{k_4}^{12} - \gamma_{k_4}^* U_{k_1}^{22*} U_{k_2}^{22*} U_{k_3}^{22} U_{k_4}^{12} - \gamma_{k_4} U_{k_1}^{12*} U_{k_2}^{12*} U_{k_3}^{12} U_{k_4}^{22}) \\
V^{(3)} &= \frac{-J}{4N_L} (4\gamma_{k_4-k_2} U_{k_1}^{12*} U_{k_2}^{22*} U_{k_3}^{11} U_{k_4}^{22} + 4\gamma_{k_3-k_2} U_{k_1}^{12*} U_{k_2}^{22*} U_{k_3}^{21} U_{k_4}^{12} - 2\gamma_{k_1} U_{k_1}^{12*} U_{k_2}^{22*} U_{k_3}^{21} U_{k_4}^{22} - 2\gamma_{k_1}^* U_{k_1}^{22*} U_{k_2}^{12*} U_{k_3}^{11} U_{k_4}^{12} \\
&\quad - \gamma_{k_4}^* U_{k_1}^{22*} U_{k_2}^{22*} U_{k_3}^{21} U_{k_4}^{12} - \gamma_{k_3}^* U_{k_1}^{22*} U_{k_2}^{22*} U_{k_3}^{11} U_{k_4}^{22} - \gamma_{k_4} U_{k_1}^{12*} U_{k_2}^{12*} U_{k_3}^{11} U_{k_4}^{22} - \gamma_{k_3} U_{k_1}^{12*} U_{k_2}^{12*} U_{k_3}^{21} U_{k_4}^{12}) \\
V^{(4)} &= \frac{-J}{4N_L} (4\gamma_{k_4-k_2} U_{k_1}^{11*} U_{k_2}^{21*} U_{k_3}^{11} U_{k_4}^{22} + 4\gamma_{k_3-k_2} U_{k_1}^{11*} U_{k_2}^{21*} U_{k_3}^{21} U_{k_4}^{12} - 2\gamma_{k_1} U_{k_1}^{11*} U_{k_2}^{21*} U_{k_3}^{21} U_{k_4}^{22} - 2\gamma_{k_1}^* U_{k_1}^{21*} U_{k_2}^{11*} U_{k_3}^{11} U_{k_4}^{12} \\
&\quad - \gamma_{k_4}^* U_{k_1}^{21*} U_{k_2}^{21*} U_{k_3}^{21} U_{k_4}^{12} - \gamma_{k_3}^* U_{k_1}^{21*} U_{k_2}^{21*} U_{k_3}^{11} U_{k_4}^{22} - \gamma_{k_4} U_{k_1}^{11*} U_{k_2}^{11*} U_{k_3}^{11} U_{k_4}^{22} - \gamma_{k_3} U_{k_1}^{11*} U_{k_2}^{11*} U_{k_3}^{21} U_{k_4}^{12}) \\
V^{(5)} &= \frac{-J}{4N_L} (4\gamma_{k_4-k_2} U_{k_1}^{12*} U_{k_2}^{21*} U_{k_3}^{12} U_{k_4}^{21} + 4\gamma_{k_3-k_2} U_{k_1}^{12*} U_{k_2}^{21*} U_{k_3}^{22} U_{k_4}^{11} + 4\gamma_{k_4-k_1} U_{k_1}^{22*} U_{k_2}^{11*} U_{k_3}^{12} U_{k_4}^{21} + 4\gamma_{k_3-k_1} U_{k_1}^{22*} U_{k_2}^{11*} U_{k_3}^{22} U_{k_4}^{11} \\
&\quad - 2\gamma_{k_1} U_{k_1}^{12*} U_{k_2}^{21*} U_{k_3}^{22} U_{k_4}^{21} - 2\gamma_{k_2} U_{k_1}^{12*} U_{k_2}^{22*} U_{k_3}^{11} U_{k_4}^{21} - 2\gamma_{k_1}^* U_{k_1}^{22*} U_{k_2}^{11*} U_{k_3}^{12} U_{k_4}^{11} - 2\gamma_{k_2}^* U_{k_1}^{22*} U_{k_2}^{11*} U_{k_3}^{12} U_{k_4}^{11} - 2\gamma_{k_4}^* U_{k_1}^{22*} U_{k_2}^{21*} U_{k_3}^{22} U_{k_4}^{11} \\
&\quad - 2\gamma_{k_3}^* U_{k_1}^{22*} U_{k_2}^{21*} U_{k_3}^{12} U_{k_4}^{21} - 2\gamma_{k_4} U_{k_1}^{12*} U_{k_2}^{11*} U_{k_3}^{12} U_{k_4}^{21} - 2\gamma_{k_3} U_{k_1}^{12*} U_{k_2}^{11*} U_{k_3}^{22} U_{k_4}^{11}) \\
V^{(6)} &= \frac{-J}{4N_L} (4\gamma_{k_4-k_2} U_{k_1}^{12*} U_{k_2}^{22*} U_{k_3}^{11} U_{k_4}^{21} - \gamma_{k_1} U_{k_1}^{12*} U_{k_2}^{22*} U_{k_3}^{21} U_{k_4}^{21} - \gamma_{k_1}^* U_{k_1}^{22*} U_{k_2}^{12*} U_{k_3}^{11} U_{k_4}^{11} - \gamma_{k_4}^* U_{k_1}^{22*} U_{k_2}^{22*} U_{k_3}^{21} U_{k_4}^{11} - \gamma_{k_4} U_{k_1}^{12*} U_{k_2}^{12*} U_{k_3}^{11} U_{k_4}^{21}) \\
V^{(7)} &= \frac{-J}{4N_L} (4\gamma_{k_4-k_2} U_{k_1}^{11*} U_{k_2}^{21*} U_{k_3}^{12} U_{k_4}^{22} - \gamma_{k_1} U_{k_1}^{11*} U_{k_2}^{21*} U_{k_3}^{22} U_{k_4}^{22} - \gamma_{k_1}^* U_{k_1}^{21*} U_{k_2}^{11*} U_{k_3}^{12} U_{k_4}^{11} - \gamma_{k_4}^* U_{k_1}^{22*} U_{k_2}^{22*} U_{k_3}^{21} U_{k_4}^{12} - \gamma_{k_4} U_{k_1}^{11*} U_{k_2}^{11*} U_{k_3}^{12} U_{k_4}^{22}) \\
V^{(8)} &= \frac{-J}{4N_L} (4\gamma_{k_4-k_2} U_{k_1}^{12*} U_{k_2}^{21*} U_{k_3}^{12} U_{k_4}^{22} + 4\gamma_{k_4-k_1} U_{k_1}^{22*} U_{k_2}^{11*} U_{k_3}^{12} U_{k_4}^{22} - \gamma_{k_1} U_{k_1}^{12*} U_{k_2}^{21*} U_{k_3}^{22} U_{k_4}^{22} - \gamma_{k_2} U_{k_1}^{22*} U_{k_2}^{11*} U_{k_3}^{22} U_{k_4}^{22} - \gamma_{k_1}^* U_{k_1}^{22*} U_{k_2}^{11*} U_{k_3}^{12} U_{k_4}^{22} \\
&\quad - \gamma_{k_2}^* U_{k_1}^{12*} U_{k_2}^{21*} U_{k_3}^{12} U_{k_4}^{22} - 2\gamma_{k_4}^* U_{k_1}^{22*} U_{k_2}^{21*} U_{k_3}^{22} U_{k_4}^{12} - 2\gamma_{k_4} U_{k_1}^{12*} U_{k_2}^{11*} U_{k_3}^{12} U_{k_4}^{22}) \\
V^{(9)} &= \frac{-J}{4N_L} (4\gamma_{k_4-k_2} U_{k_1}^{12*} U_{k_2}^{21*} U_{k_3}^{11} U_{k_4}^{21} + 4\gamma_{k_4-k_1} U_{k_1}^{22*} U_{k_2}^{11*} U_{k_3}^{11} U_{k_4}^{21} - \gamma_{k_1} U_{k_1}^{12*} U_{k_2}^{21*} U_{k_3}^{21} U_{k_4}^{21} - \gamma_{k_2} U_{k_1}^{22*} U_{k_2}^{11*} U_{k_3}^{21} U_{k_4}^{21} - \gamma_{k_1}^* U_{k_1}^{22*} U_{k_2}^{11*} U_{k_3}^{11} U_{k_4}^{21} \\
&\quad - \gamma_{k_2}^* U_{k_1}^{12*} U_{k_2}^{21*} U_{k_3}^{11} U_{k_4}^{21} - 2\gamma_{k_4}^* U_{k_1}^{22*} U_{k_2}^{21*} U_{k_3}^{21} U_{k_4}^{11} - 2\gamma_{k_4} U_{k_1}^{12*} U_{k_2}^{11*} U_{k_3}^{11} U_{k_4}^{21})
\end{aligned} \tag{D11}$$

We have employed the unitary transformation U :

$$U = \frac{1}{\sqrt{2}} \begin{pmatrix} \sqrt{1 + \frac{B}{A}} e^{i\frac{\phi_{\mathbf{k}}}{2}} & \sqrt{1 - \frac{B}{A}} e^{i\frac{\phi_{\mathbf{k}}}{2}} \\ \sqrt{1 - \frac{B}{A}} e^{-i\frac{\phi_{\mathbf{k}}}{2}} & -\sqrt{1 + \frac{B}{A}} e^{-i\frac{\phi_{\mathbf{k}}}{2}} \end{pmatrix} \tag{D12}$$

-
- [1] K. S. Novoselov, A. K. Geim, S. V. Morozov, D. Jiang, M. I. Katsnelson, I. V. Grigorieva, S. V. Dubonos, and A. A. Firsov, *Nature* **438**, 197 (2005).
- [2] A. De Martino, L. Dell'Anna, and R. Egger, *Phys. Rev. Lett.* **98**, 066802 (2007).
- [3] C.-H. Park, L. Yang, Y.-W. Son, M. L. Cohen, and S. G. Louie, *Phys. Rev. Lett.* **101**, 126804 (2008).
- [4] C.-H. Park, L. Yang, Y.-W. Son, M. L. Cohen, and S. G. Louie, *Nature Physics* **4**, 213 (2008).
- [5] X.-Z. Yan and C. S. Ting, *Phys. Rev. Lett.* **101**, 126801 (2008).
- [6] L. Zhu, R. Ma, L. Sheng, M. Liu, and D.-N. Sheng, *Phys. Rev. Lett.* **104**, 076804 (2010).
- [7] A. H. Castro Neto, F. Guinea, N. M. R. Peres, K. S. Novoselov, and A. K. Geim, *Rev. Mod. Phys.* **81**, 109 (2009).
- [8] S. Borisenko, Q. Gibson, D. Evtushinsky, V. Zabolotnyy, B. Büchner, and R. J. Cava, *Phys. Rev. Lett.* **113**, 027603 (2014).
- [9] H. Sun and J. Zhao, *Sci. China: Phys. Mech. Astron.* **59**, 107011 (2016).
- [10] H. Sun, B. Li, and J. Zhao, *J. Phys. Condens. Matter* **28**, 425301 (2016).
- [11] A. V. Chumak, V. I. Vasyuchka, A. A. Serga, and B. Hillebrands, *Nat. Phys.* **11**, 453 (2015).
- [12] J. Fransson, A. M. Black-Schaffer, and A. V. Balatsky, *Phys. Rev. B* **94**, 075401 (2016).
- [13] H. Sun, P. Sengupta, D. Nam, and B. Yang, *Phys. Rev. B* **103**, L140404 (2021).
- [14] Z.-F. Xu, L. You, A. Hemmerich, and W. V. Liu, *Phys. Rev. Lett.* **117**, 085301 (2016).
- [15] S. S. Pershoguba, S. Banerjee, J. C. Lashley, J. Park, H. Ågren, G. Aepli, and A. V. Balatsky, *Phys. Rev. X* **8**, 011010 (2018).
- [16] Y. F. Cheng, O. Cépas, P. W. Leung, and T. Ziman, *Phys. Rev. B* **75**, 144422 (2007).
- [17] L.-H. Wu and X. Hu, *Phys. Rev. Lett.* **114**, 223901 (2015).
- [18] L. Lu, C. Fang, L. Fu, S. G. Johnson, J. D. Joannopoulos, and M. Soljačić, *Nature Physics* **12**, 337 (2016).
- [19] P. Wang, L. Lu, and K. Bertoldi, *Phys. Rev. Lett.* **115**, 104302 (2015).
- [20] L. Zhang, J. Ren, J.-S. Wang, and B. Li, *Phys. Rev. B* **87**, 144101 (2013).

- [21] S. A. Owerre, *J. Phys. Condens. Matter* **28**, 386001 (2016).
- [22] W. Cai, J. Han, F. Mei, Y. Xu, Y. Ma, X. Li, H. Wang, Y. P. Song, Z.-Y. Xue, Z.-q. Yin, S. Jia, and L. Sun, *Phys. Rev. Lett.* **123**, 080501 (2019).
- [23] L. Chen, J.-H. Chung, B. Gao, T. Chen, M. B. Stone, A. I. Kolesnikov, Q. Huang, and P. Dai, *Phys. Rev. X* **8**, 041028 (2018).
- [24] Z. Cai, S. Bao, Z.-L. Gu, Y.-P. Gao, Z. Ma, Y. Shangguan, W. Si, Z.-Y. Dong, W. Wang, Y. Wu, D. Lin, J. Wang, K. Ran, S. Li, D. Adroja, X. Xi, S.-L. Yu, X. Wu, J.-X. Li, and J. Wen, *Phys. Rev. B* **104**, L020402 (2021).
- [25] T. H. Nguyen, J. Son, S. Kim, H. Cho, C. H. Kim, Y. P. Wang, K. S. Burch, I.-S. Yang, J. Jeong, J.-G. Park, S. J. Moon, and T. W. Noh, *Phys. Rev. Lett.* **127**, 267203 (2021).
- [26] P. A. McClarty, *Annu. Rev. Condens. Matter Phys.* **13**, null (2022).
- [27] M. Hirschberger, R. Chisnell, Y. S. Lee, and N. P. Ong, *Phys. Rev. Lett.* **115**, 106603 (2015).
- [28] B. Yuan, I. Khait, G.-J. Shu, F. C. Chou, M. B. Stone, J. P. Clancy, A. Paramakanti, and Y.-J. Kim, *Phys. Rev. X* **10**, 011062 (2020).
- [29] A. Mook, K. Plekhanov, J. Klinovaja, and D. Loss, *Phys. Rev. X* **11**, 021061 (2021).
- [30] M. E. Zhitomirsky and A. L. Chernyshev, *Rev. Mod. Phys.* **85**, 219 (2013).
- [31] D. C. Elias, R. V. Gorbachev, A. S. Mayorov, S. V. Morozov, A. A. Zhukov, P. Blake, L. A. Ponomarenko, I. V. Grigorieva, K. S. Novoselov, F. Guinea, and A. K. Geim, *Nat. Phys.* **7**, 701 (2011).
- [32] D. Malz, J. Knolle, and A. Nunnenkamp, *Nat. Commun.* **10**, 3937 (2019).
- [33] Y. Onose, T. Ideue, H. Katsura, Y. Shiomi, N. Nagaosa, and Y. Tokura, *Science* **329**, 297 (2010).
- [34] T. Holstein and H. Primakoff, *Phys. Rev.* **58**, 1098 (1940).
- [35] N. D. Mermin and H. Wagner, *Phys. Rev. Lett.* **17**, 1133 (1966).
- [36] A. Kamimaki, S. Iihama, K. Suzuki, N. Yoshinaga, and S. Mizukami, *Phys. Rev. Applied* **13**, 044036 (2020).
- [37] L. Tarruell, D. Greif, T. Uehlinger, G. Jotzu, and T. Esslinger, *Nature* **483**, 302 (2012).
- [38] J. Feilhaber, W. Apel, and L. Schweitzer, *Phys. Rev. B* **92**, 245424 (2015).
- [39] J. M. Kim, M. F. Haque, E. Y. Hsieh, S. M. Nahid, I. Zarin, K.-Y. Jeong, J.-P. So, H.-G. Park, and S. Nam, *Adv. Mater.* **n/a**, 2107362 (2021).
- [40] A. Gianfrate, O. Bleu, L. Dominici, V. Ardizzone, M. De Giorgi, D. Ballarini, G. Lerario, K. W. West, L. N. Pfeiffer, D. D. Solnyshkov, D. Sanvitto, and G. Malpuech, *Nature* **578**, 381 (2020).
- [41] L. Braicovich, J. van den Brink, V. Bisogni, M. M. Sala, L. J. P. Ament, N. B. Brookes, G. M. De Luca, M. Salluzzo, T. Schmitt, V. N. Strocov, and G. Ghiringhelli, *Phys. Rev. Lett.* **104**, 077002 (2010).
- [42] E. J. Samuelsen, R. Silbergliitt, G. Shirane, and J. P. Remeika, *Phys. Rev. B* **3**, 157 (1971).
- [43] J. Cenker, B. Huang, N. Suri, P. Thijssen, A. Miller, T. Song, T. Taniguchi, K. Watanabe, M. A. McGuire, D. Xiao, and X. Xu, *Nat. Phys.* **17**, 20 (2021).
- [44] V. L. Sobolev, H. L. Huang, Y. G. Pashkevich, M. M. Larionov, I. M. Vitebsky, and V. A. Blinkin, *Phys. Rev. B* **49**, 1170 (1994).
- [45] Y.-S. Lu, J.-L. Li, and C.-T. Wu, *Phys. Rev. Lett.* **127**, 217202 (2021).
- [46] J. Wang, J. Cano, A. J. Millis, Z. Liu, and B. Yang, *Phys. Rev. Lett.* **127**, 246403 (2021).
- [47] M. Claassen, C. H. Lee, R. Thomale, X.-L. Qi, and T. P. Devereaux, *Phys. Rev. Lett.* **114**, 236802 (2015).
- [48] M. P. A. Fisher, P. B. Weichman, G. Grinstein, and D. S. Fisher, *Phys. Rev. B* **40**, 546 (1989).
- [49] A. Julku, G. M. Bruun, and P. Törmä, *Phys. Rev. B* **104**, 144507 (2021).
- [50] A. Julku, G. M. Bruun, and P. Törmä, *Phys. Rev. Lett.* **127**, 170404 (2021).
- [51] J.-A. Yang, N. Pellatz, T. Wolf, R. Nandkishore, and D. Reznik, *Nat. Commun.* **11**, 2548 (2020).
- [52] A. V. Chumak, G. A. Melkov, V. E. Demidov, O. Dzyapko, V. L. Safonov, and S. O. Demokritov, *Phys. Rev. Lett.* **102**, 187205 (2009).
- [53] J. Romhányi, K. Penc, and R. Ganesh, *Nat. Commun.* **6**, 6805 (2015).
- [54] R. Matsumoto and S. Murakami, *Phys. Rev. Lett.* **106**, 197202 (2011).